TU Delft

Delft University of Technology

Review of Performance of Advanced High Strength Steels under Impact

Xia, Peikang; Sabirov, Ilchat; Petrov, Roumen; Verleysen, Patricia

DOI
10.1002/adem.202402016

Publication date
2025

Document Version
Final published version

Published in
Advanced Engineering Materials

Citation (APA)
Xia, P., Sabirov, I., Petrov, R., & Verleysen, P. (2025). Review of Performance of Advanced High Strength Steels under Impact. *Advanced Engineering Materials*, Article 2402016. https://doi.org/10.1002/adem.202402016

Important note
To cite this publication, please use the final published version (if applicable).
Please check the document version above.

Copyright
Other than for strictly personal use, it is not permitted to download, forward or distribute the text or part of it, without the consent of the author(s) and/or copyright holder(s), unless the work is under an open content license such as Creative Commons.

Takedown policy
Please contact us and provide details if you believe this document breaches copyrights.
We will remove access to the work immediately and investigate your claim.

This work is downloaded from Delft University of Technology.
For technical reasons the number of authors shown on this cover page is limited to a maximum of 10.

Green Open Access added to TU Delft Institutional Repository

'You share, we take care!' - Taverne project

https://www.openaccess.nl/en/you-share-we-take-care

Otherwise as indicated in the copyright section: the publisher is the copyright holder of this work and the author uses the Dutch legislation to make this work public.

Check for updates

ADVANCED ENGINEERING MATERIALS
www.aem-journal.com

Review of Performance of Advanced High Strength Steels under Impact

Peikang Xia, Ilchat Sabirov,* Roumen Petrov, and Patricia Verleysen*

Three generations of advanced high strength steels (AHSS) have attracted considerable attention due to their excellent mechanical properties and relatively low cost. While there has been extensive research on the basic mechanical properties of AHSS, the impact energy absorption capacity, a critical property for ensuring passenger safety, has not been systematically investigated. In addition, the absence of standardized impact testing protocols for materials or structures hinders the comparison of results across different studies. The present review aims to provide a comparative analysis of the impact performance of thin-walled structures and sheet specimens made from the three generations of AHSS. First, an introduction to the background of AHSS is presented. Widely used experimental techniques and specimen geometries are then reviewed. This is followed by a detailed review of recent relevant studies on the first, second, and third generations of AHSS. Emphasis is placed on investigating the influence of microstructure on impact performance and the underlying mechanisms governing high-strain-rate plastic deformation under impact loading. Various strategies to improve the impact performance of AHSS are also discussed.

1. Introduction

The safety of passenger cars is significantly influenced by the materials used in their components, particularly the car body. Car components must ensure sufficient crash resistance to protect occupants during collisions, while simultaneously addressing the need for reduced vehicle weight to enhance fuel efficiency. Studies indicate that a 10% reduction in vehicle weight can improve fuel economy by ≈5.5%,[1] which also contributes to lowering CO_2 emissions.[2] However, since occupant safety cannot be compromised, the potential impact of lightweighting on crash energy absorption must be carefully evaluated. Lightweight materials, such as aluminum alloys and fiber-reinforced polymer composites, have been developed and successfully used in car components to achieve high safety standards, reduced body weight, and improved fuel efficiency. Despite these advancements, steel remains the most important material in passenger car manufacturing for three main reasons: 1) steel is significantly more affordable than composites and aluminum alloys; 2) steel has superior recyclability compared to fiber composites; and 3) steel car components are easier to repair after minor-to-moderate damage compared to fiber composites and even aluminum alloys.

The development of advanced high strength steels (AHSS) has become a key and effective strategy to meet the dual demands of crashworthiness and lightweighting in the automotive industry. AHSS represent a diverse family of steels broadly categorized into three generations.[3] 1) The first-generation AHSS include dual-phase (DP) steels, transformation-induced plasticity (TRIP) steels, complex-phase (CP) steels, and martensitic (MART) steels. They typically have a limited content of alloying elements and can be easily processed on industrial lines. The DP steels are typically obtained via intercritical annealing followed by rapid quenching resulting in the formation of ferritic–martensitic microstructure.[4] The typical microstructure of DP steels consists of soft ferrite and hard martensite. TRIP steels are processed via intercritical annealing followed by rapid quenching and holding at a temperature at which a bainitic isothermal transformation takes place and retained austenite (RA) is stabilized by enriching it with carbon.[5] TRIP steels typically have a matrix of ferrite, with RA, martensite, and bainite present in varying amounts. Controlled cooling after hot rolling or annealing to form a highly complex microstructure is typically employed for CP steels which generally feature a ferrite/bainite matrix with a minor fraction of RA, MART, and/or pearlite.[6] The MART steels are heat treated via rapid quenching to form martensite which is often followed by tempering to improve toughness and reduce brittleness.[7] Thermomechanical processing and chemical composition of these steels may also be optimized to refine grain size and improve final mechanical properties. 2) The second-generation AHSS include twinning-induced plasticity (TWIP) steels, austenitic stainless steels (AUST SS), and lightweight steel with induced

P. Xia,[+] I. Sabirov
IMDEA Materials Institute
Calle Eric Kandel 2, Getafe, 28906 Madrid, Spain
E-mail: peikang.xia@sjtu.edu.cn; ilchat.sabirov@imdea.org
R. Petrov, P. Verleysen
Research Group Materials Science and Technology
Department of Electromechanical, Systems & Metal Engineering
Ghent University
Technologiepark 46, 9052 Ghent, Belgium
R. Petrov
Department of Materials Science and Engineering
Delft University of Technology
Mekelweg 2, 2628 CD Delft, The Netherlands
The ORCID identification number(s) for the author(s) of this article can be found under https://doi.org/10.1002/adem.202402016.
[+]Present address: State Key Laboratory of Metal Matrix Composites, Shanghai Jiao Tong University, Shanghai 200240, China

DOI: 10.1002/adem.202402016

 © 2025 Wiley-VCH GmbH

15272648, 0, Downloaded from https://advanced.onlinelibrary.wiley.com/doi/10.1002/adem.202402016 by Technical University Delft, Wiley Online Library on [04/03/2025]. See the Terms and Conditions (https://onlinelibrary.wiley.com/terms-and-conditions) on Wiley Online Library for rules of use; OA articles are governed by the applicable Creative Commons License

plasticity (LI-P). These steels exhibit higher costs due to the high content (up to 30 wt%) of relatively expensive alloying elements (such as Mn) and are more challenging to process compared to the first generation. The TWIP and AUST SS are typically austenitic and undergo recrystallization heat treatment after cold rolling.[8] The LI-P steels can be classified into three categories: 1) austenite-based, 2) ferrite-based, and 3) "austenite + ferrite" duplex steels, depending on their matrix,[3] and heat treatment parameters are adjusted for each case. 3) The third-generation AHSS, with quenching and partitioning (Q&P) steels and medium-manganese (medium-Mn) steels as candidates, is still under development. These steels contain less Mn (3–12 wt%). Heat treatments applied to these steels focus on stabilizing RA and refining microstructure. For example, the Q&P treatment is applied, by first austenitizing or intercritically annealing it. This is followed by quenching to a temperature below the martensite start temperature but above the martensite finish temperature. Partitioning is then carried out at this temperature or at a higher one to enrich the untransformed austenite with carbon diffusing from the supersaturated MART.[9] This heat treatment results in a complex microstructure consisting of a tempered martensitic matrix containing a high fraction of RA and some minor amount of untempered martensite. If intercritical annealing is applied, ferrite is also present. Medium-Mn steels often contain ferrite and RA after martensite-to-austenite reversion treatment.[3]

There is widespread consensus that first-generation AHSS exhibit high strength but limited ductility, whereas second-generation AHSS offer both high strength and improved ductility. The development of the third-generation AHSS aims to bridge the property gap between the first and second generations while maintaining affordability. **Figure 1** summarizes the tensile strength and total elongation data for each generation of AHSS based on existing publications.

For evaluating energy absorption, the area under the engineering stress–strain curve is commonly used as a simplified measure.[10] Alternatively, derived formulae such as UTS × TE[11] or (YS + UTS) × UE/2[12] are also used, where YS, UTS, UE, and TE are yield strength, ultimate tensile strength, uniform elongation, and total elongation, respectively. In **Table 1**, we have listed the mechanical properties under tension and the derived energy absorption capacity of selected AHSS reported in the literature.

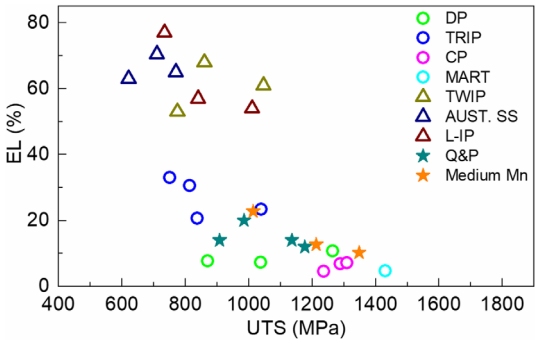

Figure 1. Ashby plot of tensile elongation versus ultimate tensile strength for various AHSS. Detailed data are provided in Table 1.

The impact energy absorption capacity of vehicles is primarily influenced by material behavior, as well as the specific design and assembly of components.[13] Thin-walled structures and sheet specimens are commonly used to evaluate the impact performance of AHSS, as they represent typical components in automotive engineering. Simulations of impact tests are frequently conducted to enhance the understanding of structural impact behavior. However, the lack of standardized testing protocols has led to variations in specimen geometries and test conditions across research laboratories globally, making comparisons of reported results challenging. Additionally, impact scenarios involve diverse and complex loading modes, including torsion, shear, bending, etc. As a result, conventional mechanical indices such as uniaxial tensile properties or fracture toughness do not provide reliable predictions of crashworthiness properties.[14,15]

The present article provides a comprehensive overview of the impact performance of three generations of AHSS, offering a novel contribution to the field. First, an analysis of the developed experimental techniques and specimen geometries used is provided. Experimental data on the impact performance of AHSS are then systematically reviewed. Particular attention is paid to the influence of microstructure and deformation mechanisms on the impact performance of AHSS. In addition, related aspects such as adiabatic heating and strain rate sensitivity are discussed. Furthermore, this review article provides a framework for considering new concepts aimed at improving the energy absorption capacity of AHSS for automotive applications. By exploring innovative concepts and technologies, this work seeks to bridge gaps in understanding and facilitate the development of next-generation AHSS. These materials are intended to retain their known strength while excelling in energy absorption during collision events.

2. Sample Geometries and Impact Testing Techniques

Large steel sheet surfaces are used in automotive parts, such as door panels, roofs, and trunk lids, while thin-walled structures are employed in components such as frontal rails, B-pillars, and beams. AHSS are widely used for thin-walled structures in vehicle bodies. In car crashes, all components must absorb as much impact energy as possible to ensure the safety of the occupants. Therefore, both flat sheet specimens and thin-walled structures are commonly used in research to study the impact performance of automotive steels.

2.1. Specimen Geometries

Flat sheet samples have the simplest geometry for studying the impact resistance of AHSS. Typically, flat sheet specimens for impact testing are square or circular in shape. The geometry of the specimen (shape, dimensions, etc.), the impactor (shape, tip radius, etc.), and the boundary conditions of the specimen have a significant effect on the test results. The impact performance of AHSS specimens, given a specific size and test setup, is assessed by measuring the maximum energy absorbed before cracking or specimen failure.[16] The lack of standardized testing protocols, together with variations in sample geometries and test

 © 2025 Wiley-VCH GmbH

Table 1. Selected mechanical properties of AHSS from three different generations in open literature.

Steel	Gen.	YS [MPa]	UTS [MPa]	UE [%]	TE [%]	(YS + UTS) × UE/2 [GPa%]	References
MART1400	1	1287	1431	4.0	4.7	5.44	[102]
CP1200	1	1056	1289	7.2	6.9	8.44	[102]
CP1400	1	902	1310	6.8	7.2	7.52	[102]
DP1200	1	673	1237	11.5	4.5	10.98	[102]
DP	1	903	1265	10.3	10.8	11.17	[39]
DP	1	445	870	7.2	7.7	4.73	[103]
DP	1	525	1037	7.1	7.3	5.55	[103]
TRIP	1	501	1039	23	23.4	17.71	[39]
TRIP	1	470	750	30	33	18.30	[49]
TRIP780	1	490	837	16.3	20.6	10.82	[104]
TRIP	1	360	813	24.0	30.6	14.08	[105]
TWIP	2	524	1046	58	61	45.53	[106]
TWIP	2	430	860	60	68	38.70	[107]
TWIP	2	230	600	84	90	34.86	[108]
TWIP	2	525	775	48	53	31.20	[108]
AUST SS 301	2	225	710	56	70.5	26.18	[109]
AUST SS 316	2	356	621	53	63	25.89	[110]
AUST SS 304	2	276	770	57	65	29.81	[111]
LI-P	2	750	1010	43.5	54	38.28	[112]
LI-P	2	502	734	77	77	47.59	[113]
LI-P	2	540	840	56	57	38.64	[114]
Q&P	3	451	985	17	20	12.21	[115]
Q&P	3	419	1136	12	14	9.33	[115]
Q&P	3	829	908	11	14	9.55	[115]
Q&P	3	1152	1177	9	12	10.48	[115]
Medium Mn	3	919	1014	20	22.8	19.33	[116]
Medium Mn	3	447	1213	9.5	12.7	7.89	[116]
Medium Mn	3	727	1348	6.9	10.2	7.16	[116]

configurations, contributes to significant discrepancies in reported values across studies. As a result, a direct comparison of results from different research laboratories is challenging.

Thin-walled structures play a crucial role in vehicles as load-bearing components and energy absorbers.[17] To analyze their behavior during crash events, thin-walled structures made of AHSS are often tested under impact conditions. However, as in the previous case, the absence of test standards leads to a lack of uniformity in specimen geometries, dimensions, loading methods, and test setups. The most commonly used specimen geometries are simplified versions of structures used in vehicles. Three main types of crash test specimens can be identified based on the cross-sectional profile: hat, double hat, and square, as shown in **Figure 2**.[18,19] Additionally, variants of these specimens exist.[20,21] Circular steel tubes, which are not relevant to automotive applications, are not considered in this review.

Very often, crush initiators (or triggers, a type of auxiliary deformation structure) are introduced into specimens subjected to axial impact loading in order to 1) change the deformation mode from global buckling to progressive crushing; 2) reduce the magnitude of the initial peak force; and 3) fix the location for the onset of collapse.[22] In addition, crush initiators can prevent global buckling under imperfect axial or oblique loading, increasing energy absorption capacity. These initiators can be broadly categorized into two types:[22] 1) material-based, such as locally annealed areas of lower strength; and 2) geometry-based, such as preformed imperfections (including dimples, grooves, holes, etc.) that act as stress concentrators.

2.2. Experimental Setups and Procedures

During impact testing on flat sheet specimens (see **Figure 3**), various impactors with specific masses and shapes, such as punches, spheres, and cylinders, are used.[23–25] The shape of the impactor significantly influences the following aspects. 1) The energy absorption of the sheet specimens during impact testing: Sharper-tipped impactors penetrate specimens more easily than blunt ones, resulting in lower absorbed energy values. 2) The shape of the deformed samples is an aspect, which is

© 2025 Wiley-VCH GmbH

15272648, 0, Downloaded from https://advanced.onlinelibrary.wiley.com/doi/10.1002/adem.202402016 by Technical University Delft, Wiley Online Library on [04/03/2025]. See the Terms and Conditions (https://onlinelibrary.wiley.com/terms-and-conditions) on Wiley Online Library for rules of use; OA articles are governed by the applicable Creative Commons License

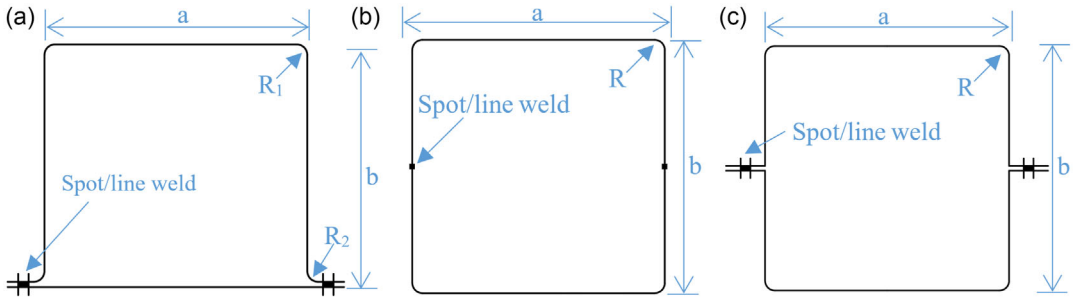

Figure 2. Different profiles of thin-walled structures used for impact testing: a) top-hat or hat-type, b) square-type, and c) double-hat type. (a,b) Reproduced with permission.[19] Copyright 2005, Elsevier Ltd.; (c) Reproduced with permission.[18] Copyright 1998, Elsevier Science Ltd.

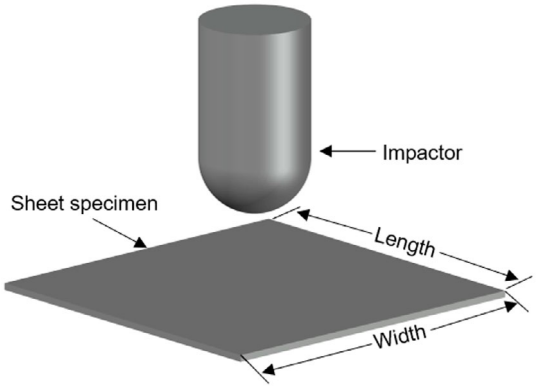

Figure 3. Schematic drawing showing impact testing of flat sheet samples. Reproduced with permission.[25] Copyright 2018, Elsevier B.V.

inherited from the shape of the impactor tip. 3) The local stress state and deformation mode during high-strain-rate plastic deformation and subsequent damage stages is important.

It should also be noted that the use of blunt impactors may result in the formation of debris, while sharp impactors are more likely to cause perforation. Additionally, the contact condition between the impactor and the specimen, specifically whether it is lubricated or dry, has a significant effect on the failure process and the amount of absorbed energy. In general, lubricated contact conditions result in higher energy absorption due to more homogeneous strain distribution and crack propagation delay.

Another critical factor is the velocity of the impactor. In flat sheet impact testing, impactors are accelerated using gravity in drop weight facilities, pneumatic force in gas gun setups, or a combination of both, depending on the facility used.[25,26] In drop weight impact test facilities, the impact speed is adjusted by changing the height of the drop mass, while in gas gun facilities, it is controlled by adjusting the gas pressure. The initial impact energy depends on the impact speed and the weight of the impactor or drop mass. In general, the impact is generated perpendicular to the sample surface, although a few cases of oblique impact have been reported.[22]

In impact testing of thin-walled structures, the impact load is typically applied in the axial direction,[19,20] although it can also be applied laterally, corresponding to bending loading,[27] or obliquely,[21] as illustrated in **Figure 4**a–c. The impact load can be generated by pneumatically or hydraulically accelerated masses[28] or by drop weights.[25] Both impact energy and impact speed can be controlled to study their influence on the impact performance of AHSS. For axial or oblique impact testing, the impactors/striking objects usually have flat contact surfaces, as shown in Figure 4b,c.

2.3. Impact Response

During impact tests on flat sheet specimens, plastic deformation and damage develop under complex stress states involving combined tension, shearing, and bending. The deformation modes are strongly influenced by the shape of the impactor used. Depending on impact energy and the shape of the impactor, cracks or even penetration of the tested specimen may occur.

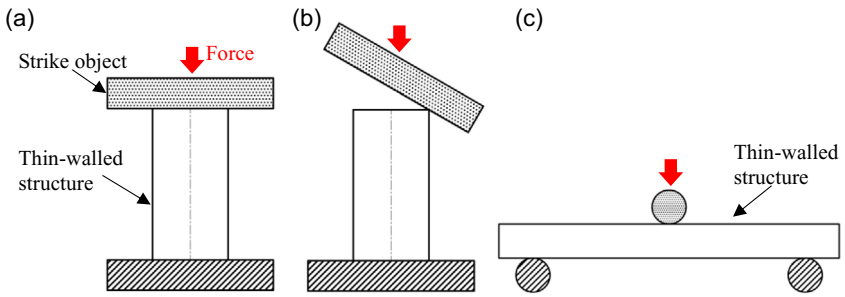

Figure 4. Schematics of impact testing on thin-walled structures with different loading conditions: a) axial impact, b) oblique impact, and c) lateral impact/bending. Reproduced with permission.[100] Copyright 2017, Elsevier Ltd.

© 2025 Wiley-VCH GmbH

15272648, 0, Downloaded from https://advanced.onlinelibrary.wiley.com/doi/10.1002/adem.202402016 by Technical University Delft, Wiley Online Library on [04/03/2025]. See the Terms and Conditions (https://onlinelibrary.wiley.com/terms-and-conditions) on Wiley Online Library for rules of use; OA articles are governed by the applicable Creative Commons License

Additionally, the local stress states and strain rates continuously change during the impact. Both parameters vary significantly throughout the volume of the deformed material, complicating the analysis of microstructural evolution and its dependence on impact conditions. Impact force and displacement are recorded to determine parameters such as maximum load, maximum displacement, and absorbed energy.

According to the force–displacement curves obtained in axial impact tests on thin-walled structures (e.g., Figure 7a–c), the impact response can be divided into two stages.[29] 1) Initial stage, which corresponds to the pre-collapse process, that is, up to the formation of the first fold. This stage is characterized by a peak in the force–displacement curve; 2) Secondary or steady stage, in which the structure continuously forms folds or collapses (see, e.g., Figure 13b). In the force–displacement curves, the latter stage corresponds to the stable plateau, although oscillating. The plateau is close to the mean impact load, defined as the total impact energy divided by the total displacement.

According to distorted structures after deformation, two types of collapse processes are generally identified for square structures during axial crushing:[30,31] 1) symmetric ones, which have three variants, that is, four individual lobes deforming inward, three lobes inward and one outward, or two opposite lobes inward while the other two outward, and 2) asymmetric ones, which include two variants, that is, three lobes outward and one inward, or two adjacent lobes outward while the other adjacent lobes inward. Representative paper models of an asymmetrical and symmetrical deformation mode are shown in **Figure 5**a,b, respectively. The symmetric collapse mode is preferred for several reasons. First, it ensures a more favorable load distribution as the undeformed portion of the structure remains aligned with the load axis. Additionally, it contributes to a stable and controlled energy absorption process through continuous folding deformation. In contrast, the asymmetric collapse mode has some drawbacks. In this mode, the structure is more likely to tilt or incline during deformation. This inclination introduces a bending component, which may result in global bending instead of crushing and lead to a less efficient energy absorption process compared to continuous folding.

Based on the deformation path of the flange line in square structures, two fundamental collapse elements have been identified from deformed specimens.[32] Type I involves a propagating hinge line, where material from one flange continuously transfers to the adjacent flange, causing the hinge line to move with respect to material points during the collapse of square structures, as shown in Figure 5c. Type II exhibits a stationary hinge line. In this case, the two adjacent flanges do not move, creating a fixed hinge line within the material, as shown in Figure 5d. Mathematical models have been proposed based on these two basic collapse elements to predict important quantities, such as the mean crushing force, effective crushing distance, total energy absorbed, and the characteristic features of folds and wrinkles.[16,33,34]

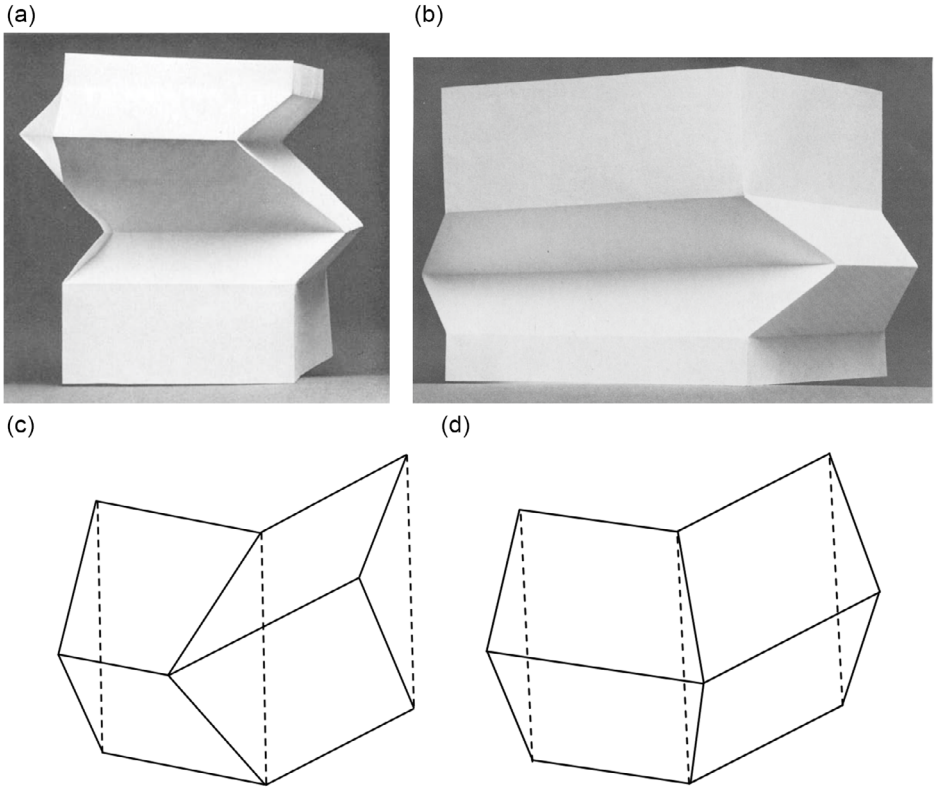

Figure 5. Paper models of simplified a) asymmetric and b) symmetric collapse modes. Reproduced with permission.[30] Copyright 1984, Elsevier Ltd. Idealized basic c) type I and d) type II collapse elements of square structures during crush testing. It should be noted that there is no one-to-one correspondence between the collapse modes and collapse elements. Reproduced with permission.[32] Copyright 1984, Elsevier Ltd.

 © 2025 Wiley-VCH GmbH

15272648, 0, Downloaded from https://advanced.onlinelibrary.wiley.com/doi/10.1002/adem.202402016 by Technical University Delft, Wiley Online Library on [04/03/2025]. See the Terms and Conditions (https://onlinelibrary.wiley.com/terms-and-conditions) on Wiley Online Library for rules of use; OA articles are governed by the applicable Creative Commons License

3. The Impact Performance of AHSS

3.1. First-Generation AHSS

The first-generation AHSS is known to have a strength × ductility product limit of 20–25 GPa%.[35] These steels have a microstructure consisting of a ferrite matrix for ductility and varying amounts of martensite, bainite, and/or RA for strength. DP, TRIP, CP, and MART steels are the main representatives of this generation. DP steel has been extensively studied for impact performance.[19,27,36–38] However, reports on CP and MART steels within this generation are limited. This gap in research highlights the need for further studies to better understand the crashworthiness and mechanical behavior of CP and MART steels, particularly in comparison to the extensively studied DP steels. Investigations that explore the influence of microstructural differences on impact performance could provide valuable insights for optimizing these materials for specific applications.

DP steels are available in a range of grades, with UTS from 500 to 1200 MPa,[39,40] tailored for different applications requiring varying levels of strength and ductility. Their versatility makes them suitable for various structural and crash-related components in vehicles. The study in ref. [36] investigated the axial crash response of thin-walled tubes made of five different steels: two DP600 steels, two high strength low alloy (HSLA) steels, and a deep drawing quality (DDQ) steel. The mechanical performance of the steels is shown in **Figure 6**a. The DP600 steel with a thickness of 1.5 mm exhibits the highest yield and ultimate tensile strength, while the DDQ steel with a thickness of 1.8 mm shows the highest ductility, despite having the lowest strength. The properties of the HSLA steels fell in between those of DP and DDQ steels. Impact experiments indicated that the studied DP steel had better impact energy absorption capability than other steels of the same thickness, for both 1.5 and 1.8 mm thicknesses. Additionally, the DP600 thin-walled structures, with a thickness of 1.5 mm, absorbed even more energy than the DDQ structures with a thickness of 1.8 mm. This indicates a promising application for lightweighting. The inclusion of multiple material types (DP, HSLA, DDQ) and thicknesses in this study allows for a comprehensive comparison of crashworthiness properties across different steel grades. However, the study did not consider the effect of thickness and weight of samples when comparing the crashworthiness of different steel grades, which may lead to inappropriate conclusions. A comparative study of DP590 and DP780 steel was reported in ref. [41], where the influence of weight and thickness on energy absorption capability were considered. Their analysis indicated that the specific energy absorption is positively affected by both weight and thickness. Another highlight of this work is that the influence of cost was also considered when evaluating the crashworthiness of different steel grades. An experimental study in ref. [37] showed that substituting HSLA340 with DP340 steel increases the energy absorption capacity of thin-walled sections by 10%. Although DP steels exhibited improved energy absorption and lightweighting potential, their significantly higher springback compared to HSLA steels poses challenges in manufacturing. These trade-offs are acknowledged but not deeply analyzed.

A study conducted in ref. [19] investigated the impact performance of both thin-walled top-hat and square structures made of DP800 steel at impact speeds of 5–15 m s^{-1}. The results showed that the initial peak load and mean force increased with increasing impact velocity, as shown in **Figure 7**. This increase could be attributed to the material's inertia and strain rate effect, which was also demonstrated by the quantitative results of numerical simulations. The study found that yield strength, section thickness, and impact speed all positively influence the mass–specific energy absorption capability. Numerical simulations showed that increasing the yield strength from 156 to 500 MPa (similar to the range from mild steel to phased steel) resulted in an average increase of ≈1 kJ kg^{-1} in the mass–specific energy absorption capacity of top-hat sections for every 100 MPa increase in yield strength. The study simulated the thickness effect using DP800 steel with varying thicknesses. The findings indicated that for every 1 mm increase in thickness, there was an average increase in mass–specific energy absorption capacity of about 4 kJ kg^{-1}. The impact performance was also tested on DP590 and DP780 steels, confirming the sensitivity of load–deformation

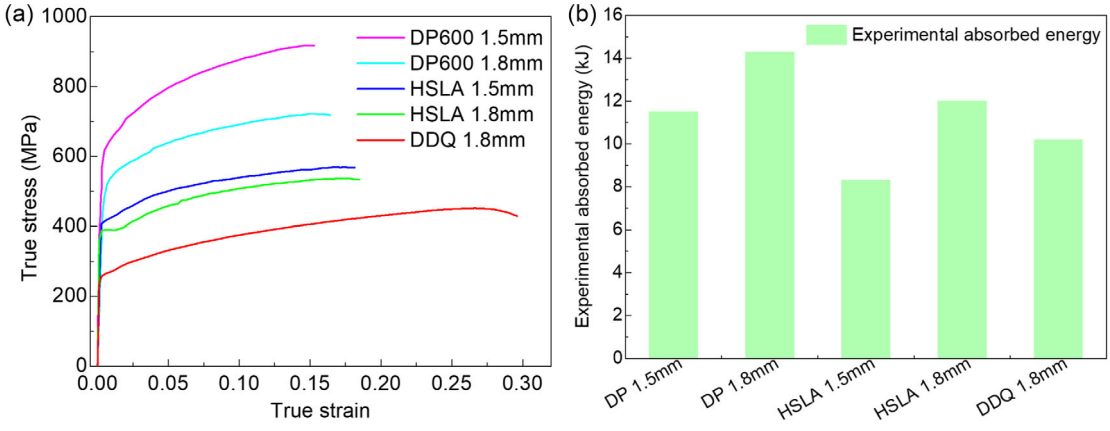

Figure 6. a) True stress–true strain curves of DP, HSLA, and DDQ steels with different thicknesses; b) experimental data on absorbed energy of the studied steels. Reproduced with permission.[36] Copyright 2009, Elsevier Ltd.

© 2025 Wiley-VCH GmbH

15272648, 0, Downloaded from https://advanced.onlinelibrary.wiley.com/doi/10.1002/adem.202402016 by Technical University Delft, Wiley Online Library on [04/03/2025]. See the Terms and Conditions (https://onlinelibrary.wiley.com/terms-and-conditions) on Wiley Online Library for rules of use; OA articles are governed by the applicable Creative Commons License

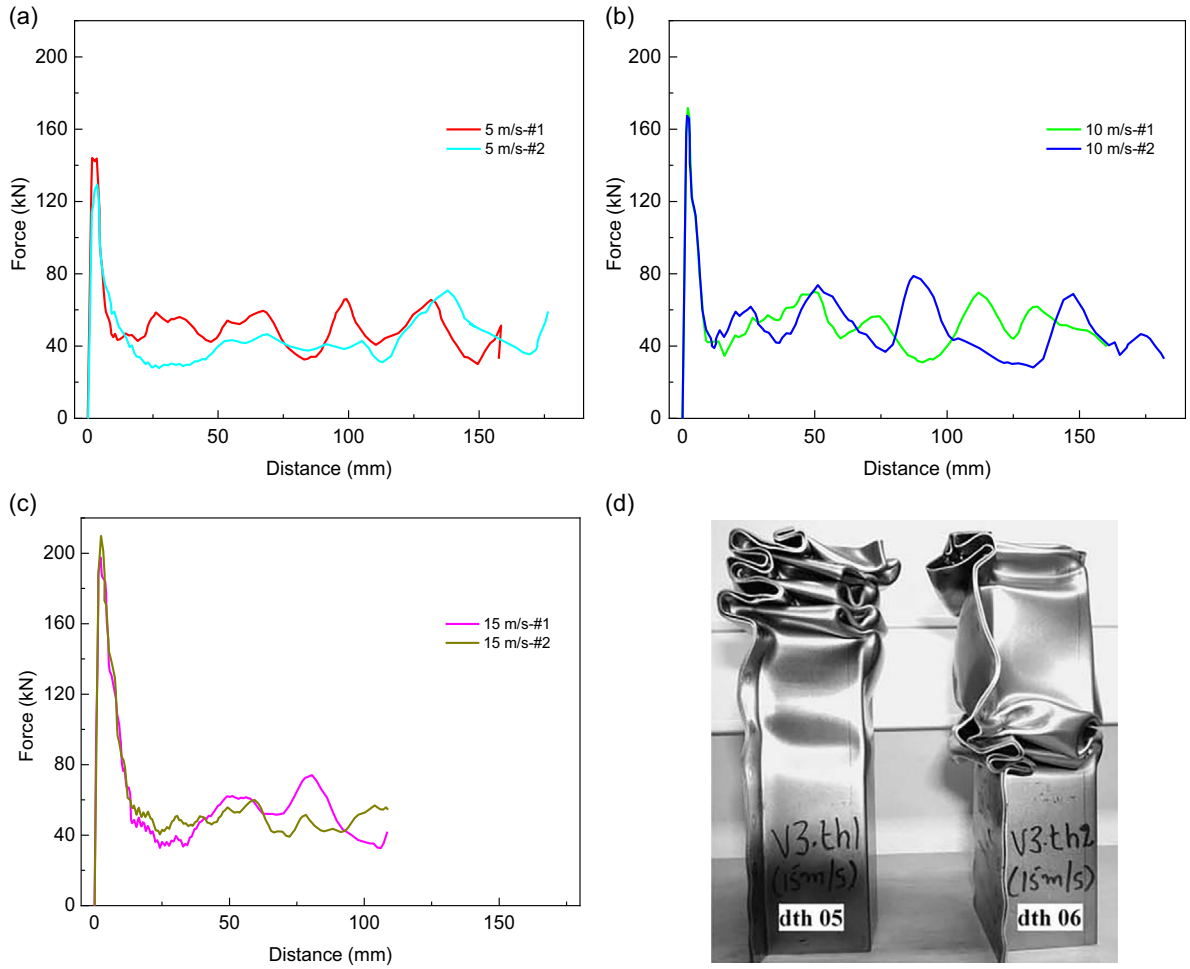

Figure 7. Smoothed force–displacement curves of top-hat structures impacted at different speeds: a) 5 m s^{-1}, b) 10 m s^{-1}, and c) 15 m s^{-1}. d) A photo of tested specimens at an impact speed of 15 m s^{-1}. Reproduced with permission.[19] Copyright 2005, Elsevier Ltd.

responses to the yield strength and thickness of the material.[42] These findings demonstrate the importance of considering material thickness in impact performance.

Additionally, studies have investigated the relationship between material properties and energy absorption in different loading scenarios. The improved energy absorption capabilities of AHSS with increasing yield strength have also been observed in lateral impact testing of thin-walled structures. For instance, the study on various steel grades, including DP, TRIP, and MART steels, with tensile strength of 270–1470 MPa, showed that the average bending moment up to a displacement of 20 mm had a linear relationship with the yield strength of the materials, as illustrated in **Figure 8**.[27] One limitation of this study is that the obtained data were not normalized by thickness, making it inconvenient to compare with results from other studies. It is important to acknowledge that the energy absorption of tested materials is also influenced by other factors, such as the forming method and geometry of thin-walled structures. For example, thin-walled structures formed through high-pressure hydroforming exhibit lower energy absorption compared to those formed through low-pressure hydroforming, as reported in ref. [36]. The authors attribute this difference to the higher thickness reduction in the high-pressure hydroforming process. High-pressure hydroforming was expected to strengthen the steel and improve its impact performance. However, experiments revealed the opposite. The possible explanation is that the strengthening effect induced by the high-pressure hydroforming process adversely affected the ductility of the thin-walled structures. The strengthening may have had a detrimental effect on the ability of the structures to withstand deformation without fracturing, which could ultimately compromise their impact performance.

While much research has focused on the crashworthiness of thin-walled structures and components, studies investigating the drop-weight impact resistance of flat-sheet specimens are relatively scarce. These investigations are crucial for understanding how material properties influence impact performance in simpler geometries, which can provide insights for broader applications. The low-velocity impact deformation process of single and multilayered DP600 steel plates was reported in ref. [43]. High-speed imaging combined with the digital image correlation (DIC) technique revealed that the plates' resistance to perforation is

© 2025 Wiley-VCH GmbH

15272648, 0, Downloaded from https://advanced.onlinelibrary.wiley.com/doi/10.1002/adem.202402016 by Technical University Delft, Wiley Online Library on [04/03/2025]. See the Terms and Conditions (https://onlinelibrary.wiley.com/terms-and-conditions) on Wiley Online Library for rules of use; OA articles are governed by the applicable Creative Commons License

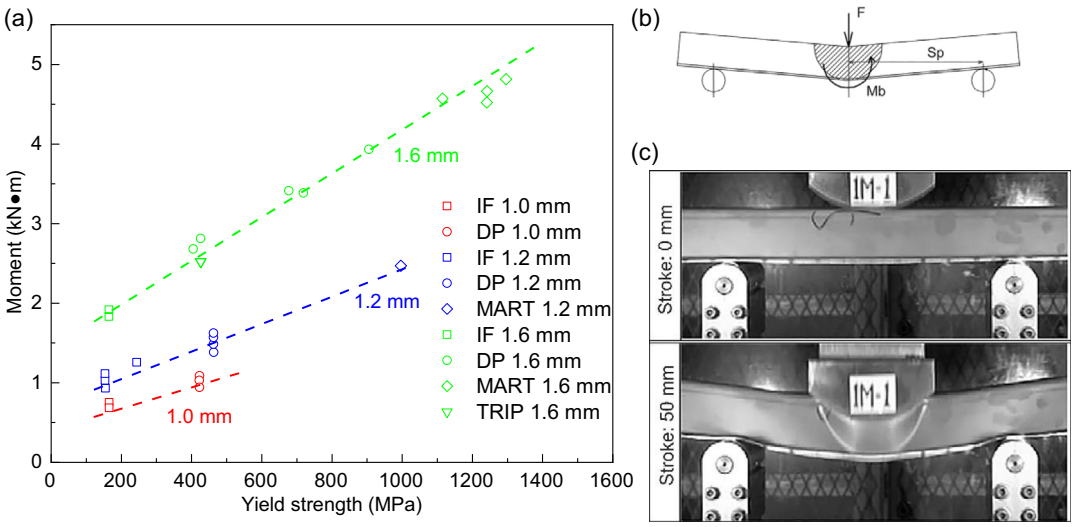

Figure 8. a) Effect of yield strength on bending moment in several AHSS (crash speed: 5 m s^{-1}; bending span: 320–470 mm), b) schematic showing of bending impact testing (F: force, Mb: moment, Sp: bending span) and c) selected images of bending impact testing at different displacements. Reproduced with permission.[27] Copyright 2012, Elsevier Ltd.

closely related to the shape of the considered impactor, such as blunt ended or ogival ended. A further study on single-layer DP600 and fully martensitic 1400M steel sheets revealed that[23] 1) the strain distribution over tested samples was significantly affected by the strain rate. The distribution of plastic strain accumulated by samples during impact testing using a hemispherical impactor was more homogeneous during quasistatic testing than during impact testing, as shown in **Figure 9**. 2) The steel with a higher tensile strength (1520 MPa) showed a more homogeneous strain distribution than the steel with a lower tensile strength (610 MPa). This difference may be attributed to the higher strain hardening capacity of the latter. The strain magnitude in the last image before fracture, as measured by DIC on DP600 steel, was in the range of 0.41–0.67, while the strain values were in the range of 0.14–0.41 on 1400M steel. This study thoroughly analyzed the strain distribution during impact deformation under different stress states. However, the influence of this strain distribution on impact energy absorption capability was not specified or discussed.

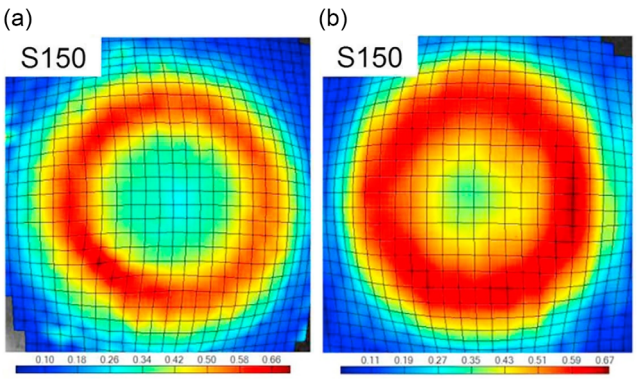

Figure 9. Equivalent plastic strain magnitude plots in the last image before fracture of selected samples during a) low-speed impact (10.5 m s^{-1}) and b) quasistatic (3×10^{-4} m s^{-1}) tests using a hemispherical impactor. Reproduced with permission.[23] Copyright 2015, Elsevier Ltd.

In another study,[44] the impact performance of DP1180 steel was experimentally studied by drop weight impact tests. A hemispherical punch was employed at impact speeds of 3–7 m s^{-1} to regulate the impact energy. The sample thickness was 1 mm, and the unclamped sample region, with a size of 314 mm^2, was free to deform. The hemispherical punch had a diameter of 16 mm. Under the conditions of the study, the impact resistance was measured to be 90 J, defined as the maximum energy absorbed before fracture. Although the DP steel had a low total elongation (8.2%) under uniaxial tension, it reached a very high true strain (81.1%) at the apex of the domed specimen, where a biaxial stress state prevailed, as shown in **Figure 10**b, when impacted with 90 J energy. Furthermore, the highest temperature resulting from adiabatic heating measured during impact testing was 225 °C, as shown in Figure 10. The primary deformation mechanisms during high-strain-rate deformation of the DP steel were dislocation glide and the formation of dislocation cells. The enhanced formability observed during drop weight impact was attributed to the high strain rate, biaxial stress state, and possible contribution from adiabatic heating.

Dislocation glide is the primary deformation mechanism for DP steels, while TRIP steels exhibit TRIP effect alongside dislocation movement. This difference leads to distinct responses under uniaxial tensile loading. However, this distinction is less evident when comparing the behavior of thin-walled structures made from these two steels. The performance of thin-walled structures made of TRIP590, TRIP780, DP780, and DP980 steels under both axial and lateral impact loading was comparatively studied in ref. [45] The results, shown in **Figure 11**, indicated that impact performance parameters, including maximum axial or lateral impact force, average impact force, and energy absorption, have a linear relationship with tensile strength. These findings agree with the theoretical model,[34] which states that

© 2025 Wiley-VCH GmbH

15272648, 0, Downloaded from https://advanced.onlinelibrary.wiley.com/doi/10.1002/adem.202402016 by Technical University Delft, Wiley Online Library on [04/03/2025]. See the Terms and Conditions (https://onlinelibrary.wiley.com/terms-and-conditions) on Wiley Online Library for rules of use; OA articles are governed by the applicable Creative Commons License

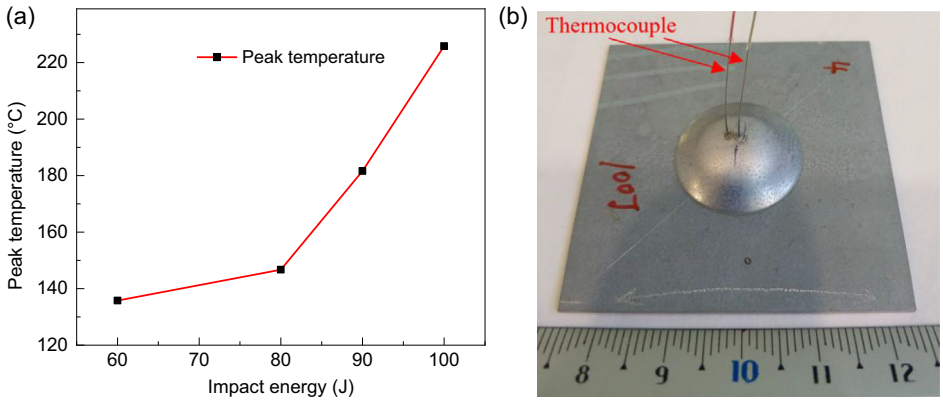

Figure 10. a) Measured peak temperature with different impact energy during drop weight impact testing on DP1180 steel sheets. b) DP1180 steel sample after impact with 100 J energy, which exceeds the impact resistance of the material resulting in crack formation. Reproduced with permission.[44] Copyright 2020, Elsevier B.V.

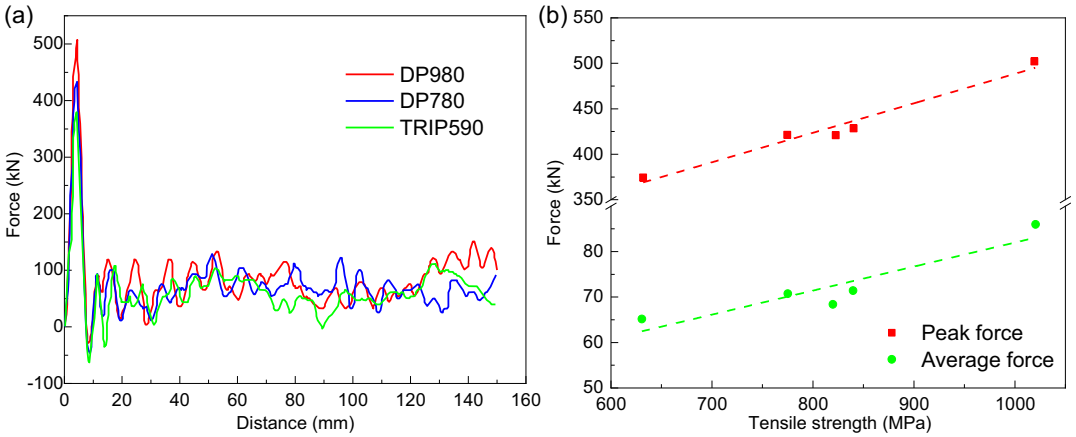

Figure 11. a) Force–displacement curves and b) relationships between tensile strength and impact force during axial impact testing on top-hat thin-walled structures. Reproduced with permission.[45] Copyright 2005, SAE International.

the crush load is proportional to the tensile strength. Additionally, high peak force/mean force ratios were observed in all tested AHSS (Figure 11), which are unfavorable and pose a threat to passenger safety. The high peak force results in high accelerations at the beginning of an impact accident, which could endanger passengers' lives unless efficient structural designs are implemented to reduce accelerations.[46] The limited strain hardening capability of the first-generation AHSS, particularly DP, MART, and CP steels, tends to exhibit high peak force/mean force ratios. This is also evident in Figure 7, although it has not been extensively studied and requires further investigation. The study in ref. [45] reported the testing results but did not account for the influence of thickness and weight when comparing the energy absorption of different steel grades.

Martensite transformation of RA under external loading, also known as the TRIP effect, has been employed to improve the ductility and strain hardening capacity of TRIP steels.[47] However, the role of the TRIP effect in the impact performance of TRIP steels is a topic of debate. In ref. [48], impact tests were conducted on 1 mm-thick square sheets of TRIP1000 steel using a conical impactor at an impact speed of 2.5–4.5 m s^{-1}. The X-ray diffraction (XRD) measurements indicated no martensite after impact testing. The absence of the TRIP effect in the study was attributed to local adiabatic heating during impact. However, it is worth noting that other studies have demonstrated the presence of the TRIP effect during high-strain-rate deformation of TRIP steels.[49,50] It is possible that the XRD technique employed to determine the martensite content in ref. [48] may have underestimated the actual fraction of martensite. The authors also studied the influence of testing temperature on the energy absorption of TRIP1000 steel. The testing results revealed that lower temperatures enhanced the energy absorption of TRIP1000 steel. For example, at an impact speed of 2.9 m s^{-1}, the impactor perforated the steel sheet at +15 °C, while it rebounded without perforation at −60 °C, as presented in **Figure 12**. However, the explanation for this phenomenon was not provided in ref. [48] One possible explanation could be attributed to the favorable conditions for the TRIP effect at lower temperatures. The TRIP effect enhances the strength and energy absorption of the steel. This correlation was demonstrated in ref. [51] where RA improved dynamic tensile mechanical properties at −40 °C due to the TRIP effect. Furthermore, the energy

© 2025 Wiley-VCH GmbH

15272648, 0, Downloaded from https://advanced.onlinelibrary.wiley.com/doi/10.1002/adem.202402016 by Technical University Delft, Wiley Online Library on [04/03/2025]. See the Terms and Conditions (https://onlinelibrary.wiley.com/terms-and-conditions) on Wiley Online Library for rules of use; OA articles are governed by the applicable Creative Commons License

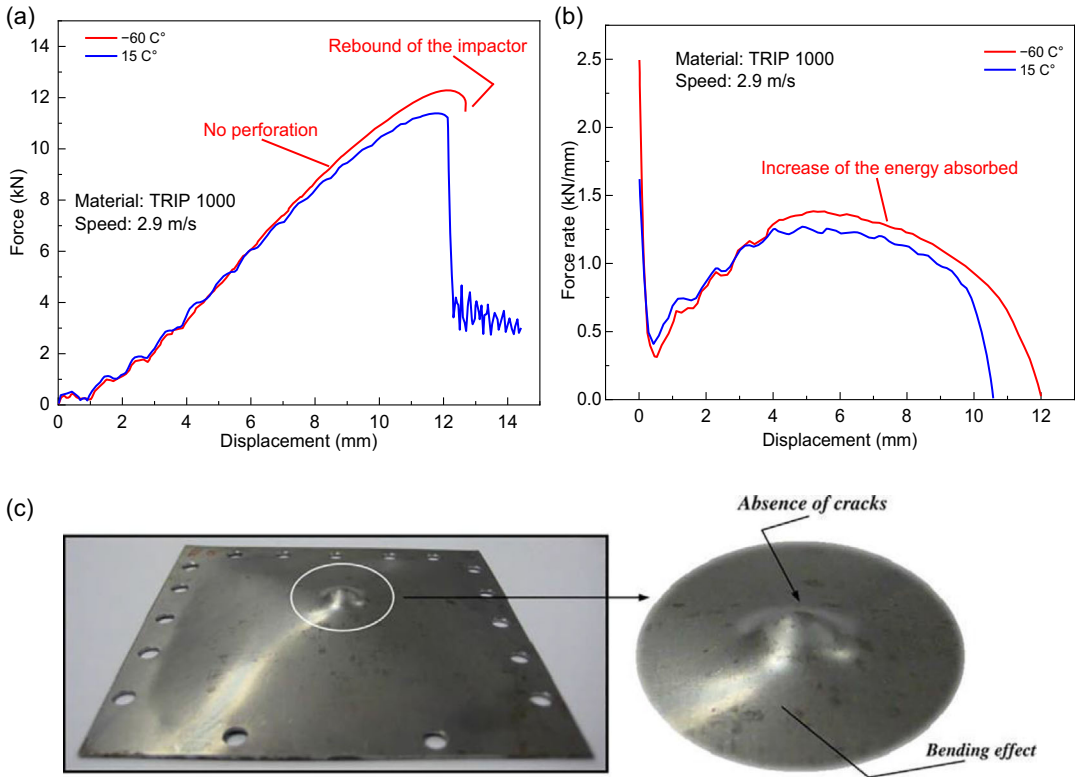

Figure 12. Evolution of a) force; b) force rate with displacement of impactor during impact testing; c) image of a specimen impacted at a speed of 2.9 m s^{-1} and a temperature of −60 °C. Reproduced with permission.[48] Copyright 2010, Elsevier Ltd.

absorption is also affected by the type of contact, whether it is lubricated or dry. In the case of lubricated contact, the failure of samples was delayed due to the absence of tangential stresses on the impactor/sheet interface. It is important to note that the contact condition did not affect the failure mode.[48]

Cold working is a commonly used method to strengthen AHSS. It has also been successful in enhancing the impact performance of TRIP780 and DP600 steels, as reported in ref. [52]. Crash testing of top-hat structures showed that those made of prestrained steels (5% and 10% for the TRIP780 steel, 4% and 8% for the DP600 steel) exhibited higher mean impact forces than those made of non-prestrained steels, even though the sheet thickness was reduced after prestraining. Furthermore, baking hardening may also be utilized to improve the impact performance of AHSS, such as TRIP780 steel, though it appears to be less efficient than prestraining. For example, quantitative analysis demonstrated that a prestraining of 10% and a baking cycle of 20 min at 170 °C increased the mean impact force by 11% and 4%, respectively. However, it should be noted that both cold working and baking treatments have a negative effect on ductility, as observed in many steels such as DP[53] and TRIP[54] steels.

3.2. Second-Generation AHSS

The second-generation AHSS are known for their excellent mechanical properties, which are characterized by a high product of strength × ductility, reaching up to 60 GPa%.[35] This largely benefits from the presence of austenite as the primary constituent in these steels. The formation of twins and/or martensite during the deformation and/or transformation of austenite, as well as their interaction with dislocations, all contribute to the improved ductility and strength properties. However, the soft nature of austenite also leads to a drawback, that is, relatively low yield strength. The main representatives of this generation are TWIP, AUST SS, and LI-P steels. It is important to note that AUST SSs have a relatively high price due to the addition of alloying elements, such as Ni and Cr, making them less attractive as crash-box material in automotive applications compared to lower-alloyed AHSS.[55] The impact performance of second-generation AHSS has primarily been studied for TWIP and AUST SS, while reports on LI-P steels remain scarce. Research on LI-P steels has largely focused on achieving an optimal balance of high strength, excellent ductility, and reduced weight to meet lightweighting objectives or to explore deformation mechanisms.[56,57] As a result, their dynamic impact performance has received comparatively less attention.

TWIP steels have received much interest in recent years due to their excellent strength and ductility. In ref. [58], a comparative study was conducted on thin-walled top-hat sections made of several AHSS, including DP590, TRIP800, DP980, TWIP1000, and prestrained TWIP1000 steels. The axial impact experiments revealed that the top-hat structures made of TWIP1000 steel exhibited a lower mean impact force than those made of DP980 steel (**Figure 13**). However, after plastic prestraining to strains of 8% and 17%, structures made of TWIP1000 showed

 © 2025 Wiley-VCH GmbH

15272648, 0, Downloaded from https://advanced.onlinelibrary.wiley.com/doi/10.1002/adem.202402016 by Technical University Delft, Wiley Online Library on [04/03/2025]. See the Terms and Conditions (https://onlinelibrary.wiley.com/terms-and-conditions) on Wiley Online Library for rules of use; OA articles are governed by the applicable Creative Commons License

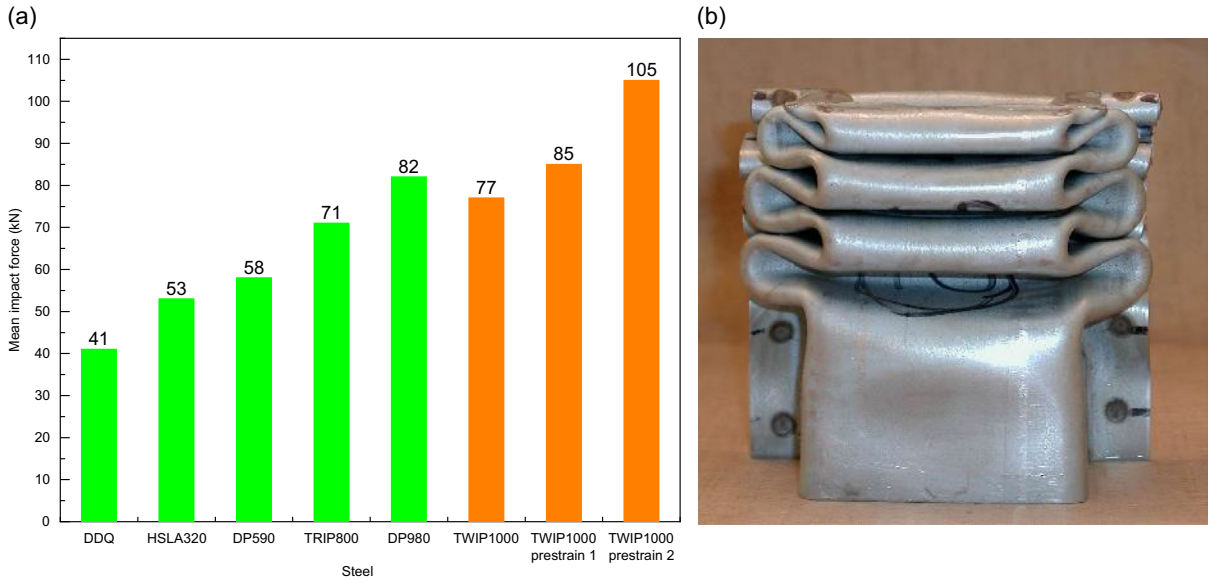

Figure 13. a) Mean impact force during testing of top-hat structures made of different AHSS; b) impacted thin-walled structure made of TWIP1000 steel at a speed 58 km h^{-1}. DDQ: deep drawing quality steel. Reproduced with permission.[58] Copyright 2005, SAE International.

the highest mean impact force, as presented in Figure 13. Unfortunately, the report does not provide a detailed explanation for the improved impact performance, nor does it clarify the differences in how the TRIP and TWIP effects influence the impact performance of steels.

Furthermore, the impact performance of TWIP steels can be improved by microstructure optimization at the stage of casting and thermomechanical processing. For example, in ref. [59], strip casting combined with cold rolling was employed to produce TWIP steel. The authors found that the thin-walled structures made through this method exhibited better impact performance than similar structures made of recrystallized TWIP780 steel and DP800 steel. Less impact distance was required to consume the same amount of impact energy (**Figure 14**a). The authors concluded that the crashworthiness of TWIP steel is intrinsically linked to its strain hardening behavior, which is determined by the combined effects of dislocation glide and deformation twinning.[60] The strain hardening behavior of TWIP steels is influenced by the stacking fault energy (SFE) of the material. In a subsequent study,[61] two additional strategies were employed to enhance the impact performance of TWIP steels: 1) recovery annealing, which tailored the strain hardening behavior and increased the yield strength of the TWIP steels as a result of the recovered austenite grains, and 2) local laser heat treatment of thin-walled structures, which generated soft/hard bands in the structure and, thus, increased the mean impact force. A similar effect to annealing, which softens the material and restores its ductility, was observed in the laser-irradiated areas, although the local microstructure in these areas was not reported. The improved impact performance was demonstrated by the shorter impact distance and higher mean impact force under the same impact conditions, as shown in Figure 14b,c.

In addition, more stable force–displacement curves were frequently observed in TWIP steels compared to DP steels. TWIP steels typically show a smaller difference between peak force and mean impact force than the latter, as shown in Figure 8 and 14. A more stable response to impact loading is favorable for both energy absorption and passenger safety. Another method for achieving "flattened" force–displacement curves is through the use of tapered thin-walled structures, as presented in ref. [62].

To control the axial crush response of box components and obtain a desired load–displacement curve, collapse initiators can be employed. In ref. [29], the authors adopted specific collapse initiators, that is, transverse grooves with full sidewall width, on square thin-walled structures made of 304 stainless steel. Quasistatic compression testing of these structures, under similar deformation modes, exhibited high consistency and repeatability in: 1) collapse mode, including consistent collapse initiation location and similar progressive folding process, and 2) mechanical behavior, such as the force–displacement curve and mean crushing force. In a follow-up study,[63] the authors demonstrated that such consistency and repeatability can also be realized in steels with varying strength, strain hardening behavior, ductility, etc. These studies demonstrated that the axial crush response can be effectively controlled, narrowing the gap between results and computer simulations, while offering valuable guidelines for automotive industry design.

The TRIP effect in AUST SS can significantly influence its deformation response. This effect is influenced by various factors, including strain rates and stress states. The TRIP effect was observed during the impact testing of 304 SS sheet specimens in ref. [64,65], where both drop weight tower and gas gun impact systems were employed to cover a wide range of impact speeds, that is, from 2.5 to ≈200 m s^{-1}. The martensite volume fraction tended to decrease with increasing impact speed. This observation is related to the temperature increase caused by adiabatic heating, which stabilizes austenite due to the increasing SFE.[65] Additionally, the energy absorption was influenced by

© 2025 Wiley-VCH GmbH

15272648, 0, Downloaded from https://advanced.onlinelibrary.wiley.com/doi/10.1002/adem.202402016 by Technical University Delft, Wiley Online Library on [04/03/2025]. See the Terms and Conditions (https://onlinelibrary.wiley.com/terms-and-conditions) on Wiley Online Library for rules of use; OA articles are governed by the applicable Creative Commons License

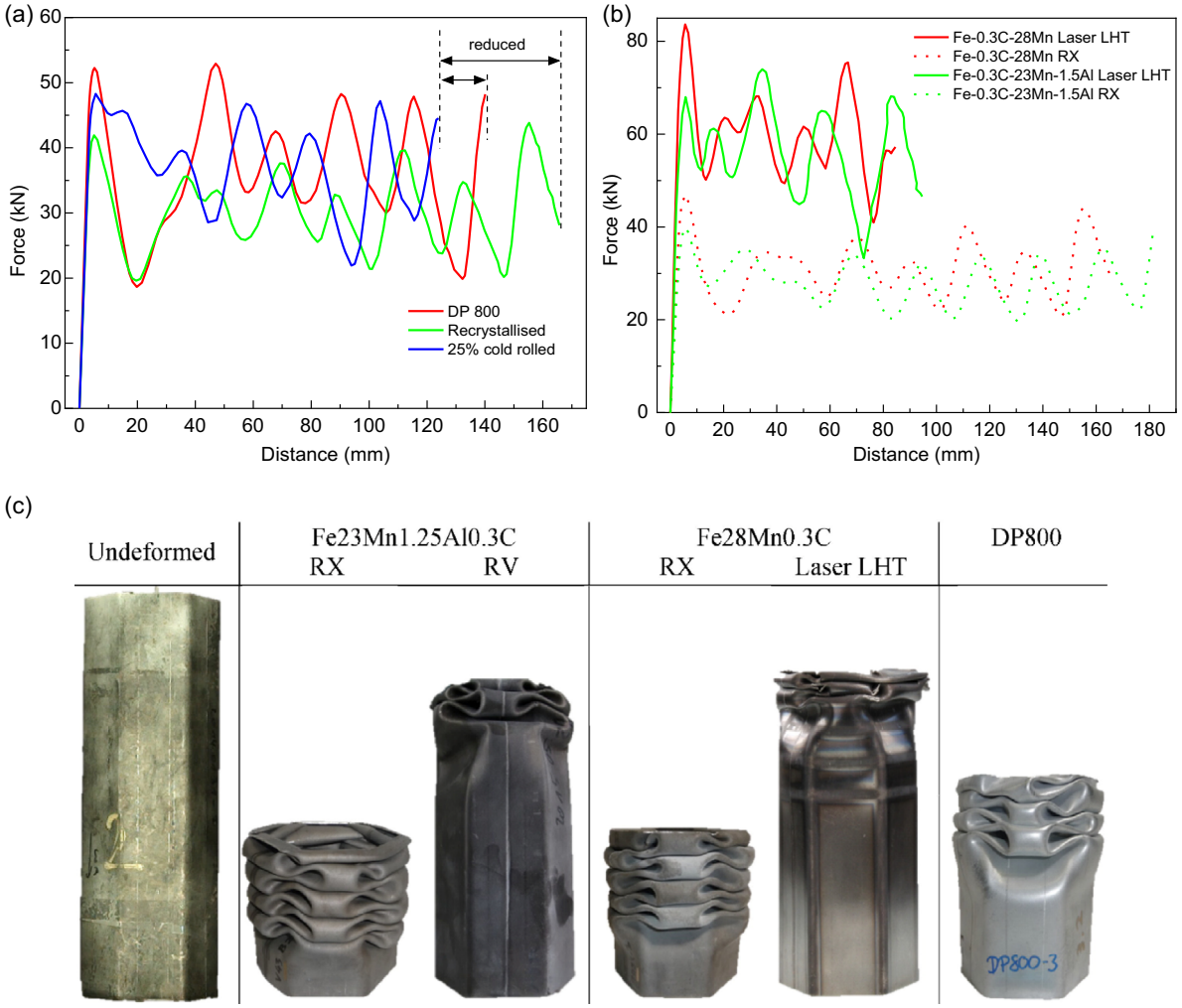

Figure 14. Force–displacement curves of top-hat structures: a) comparison between DP800 steel and Fe–0.3C–29Mn (wt%) TWIP steel under cold-rolled and recrystallized conditions. Reproduced with permission.[59] Copyright 2014, CIRP. b) Comparison between recrystallized (RX) and laser local heat-treated (laser LHT) Fe–0.3C–29Mn and Fe–0.3C–23Mn–1.5Al (wt%) TWIP steels. c) Images of thin-walled structures before and after crash testing. RV: recovery annealed. Reproduced with permission.[61] Copyright 2016, Elsevier Ltd.

the shape of the impactor used during impact testing of sheet specimens. For instance, specimens tested with sharp/conical impactors absorbed less energy than those impacted with hemispherical impactors. Further analysis indicated that the TRIP effect had minimal contribution to energy absorption when a conical impactor was used. However, the TRIP effect promoted energy absorption when hemispherical impactors were used. This difference can be attributed to the volume of deformed material and the stress states involved. When a sheet is impacted by a hemispherical impactor, a larger volume of material, including austenite, is deformed. The biaxial stress state at the top of the dome in this scenario promotes the TRIP effect.

3.3. Third-Generation AHSS

The third-generation AHSS is currently under research and development, which aims to achieve a better strength–ductility trade-off than the first generation, while also being more cost-effective than the second generation. The strength/ductility properties of these new steels are located in the property gap between the first and second generations.[35] These steels typically contain a specific proportion and distribution of RA in a bainite or martensite matrix, along with some ferrite and/or precipitates, which contribute to their enhanced properties. At present, two promising candidates for the third-generation AHSS are Q&P and medium-Mn steels due to their excellent strength and ductility performance. The list of potential candidates is expected to expand with other novel steels in the future.[3,35] As Q&P and medium-Mn steels are relatively novel and still in the process of gaining broader industrial adoption, research on their impact performance remains limited. Currently, only two publications specifically addressing the impact performance of Q&P steel have been found: one focuses on thin-walled structures, while the other investigates sheet materials. These studies are discussed in detail in this section.

© 2025 Wiley-VCH GmbH

15272648, 0, Downloaded from https://advanced.onlinelibrary.wiley.com/doi/10.1002/adem.202402016 by Technical University Delft, Wiley Online Library on [04/03/2025]. See the Terms and Conditions (https://onlinelibrary.wiley.com/terms-and-conditions) on Wiley Online Library for rules of use; OA articles are governed by the applicable Creative Commons License

The impact performance of top-hat thin-walled structures made of Q&P1080 and DP1030 steels was investigated in ref. [66] The Q&P steel exhibited ultimate tensile strength and yield strength ≈50 MPa higher than those of the DP steel. The experimental findings demonstrated that the Q&P steel had superior energy absorption capacity compared to the DP steel. When subjected to the same impactor displacement, the former exhibited higher average force and energy absorption, as depicted in **Figure 15**. The microstructure of the Q&P steel consisted of martensite, ferrite, and RA. The transformation of RA into martensite during impact deformation was confirmed through electron backscatter diffraction (EBSD) analysis. The fraction of RA decreased from its initial value of 9.9% to a minimum of 2.1% after impact deformation. The amount of RA preserved in the deformed samples varied depending on the local plastic strain. Although the study presented the crushing deformation processes, the consecutive collapse process was not observed, and the tests were not repeated. Additionally, the analysis of impact energy did not account for the weight and thickness of the tested structures. Further research is needed to address these limitations and provide more comprehensive insights.

The impact performance of sheet Q&P steel was investigated in ref. [25] using drop weight impact experiments. The Q&P steel under study featured a microstructure consisting of martensite and RA. EBSD analysis clearly demonstrated the TRIP effect, as illustrated in **Figure 16**. The study found that the fraction of RA decreased exponentially as plastic strain increased from the initial 9.6% to 1.2% after reaching a true plastic strain of 28.6% (Figure 16a,b). The tempered martensite matrix was also found to play a crucial role in accommodating plastic deformation. Equiaxed tempered MART grains were deformed into elongated grains, which facilitated the accumulation of significant plastic strain. This is evident from the kernel average misorientation (KAM) maps presented in Figure 16. Moreover, the temperature rise caused by adiabatic heating was measured during the impact tests. The highest temperature recorded was 187 °C at an impact energy of 110 J. The adiabatic heating-induced temperature rise resulted in material softening. As a result, the energy absorption during impact testing was slightly lower compared to that

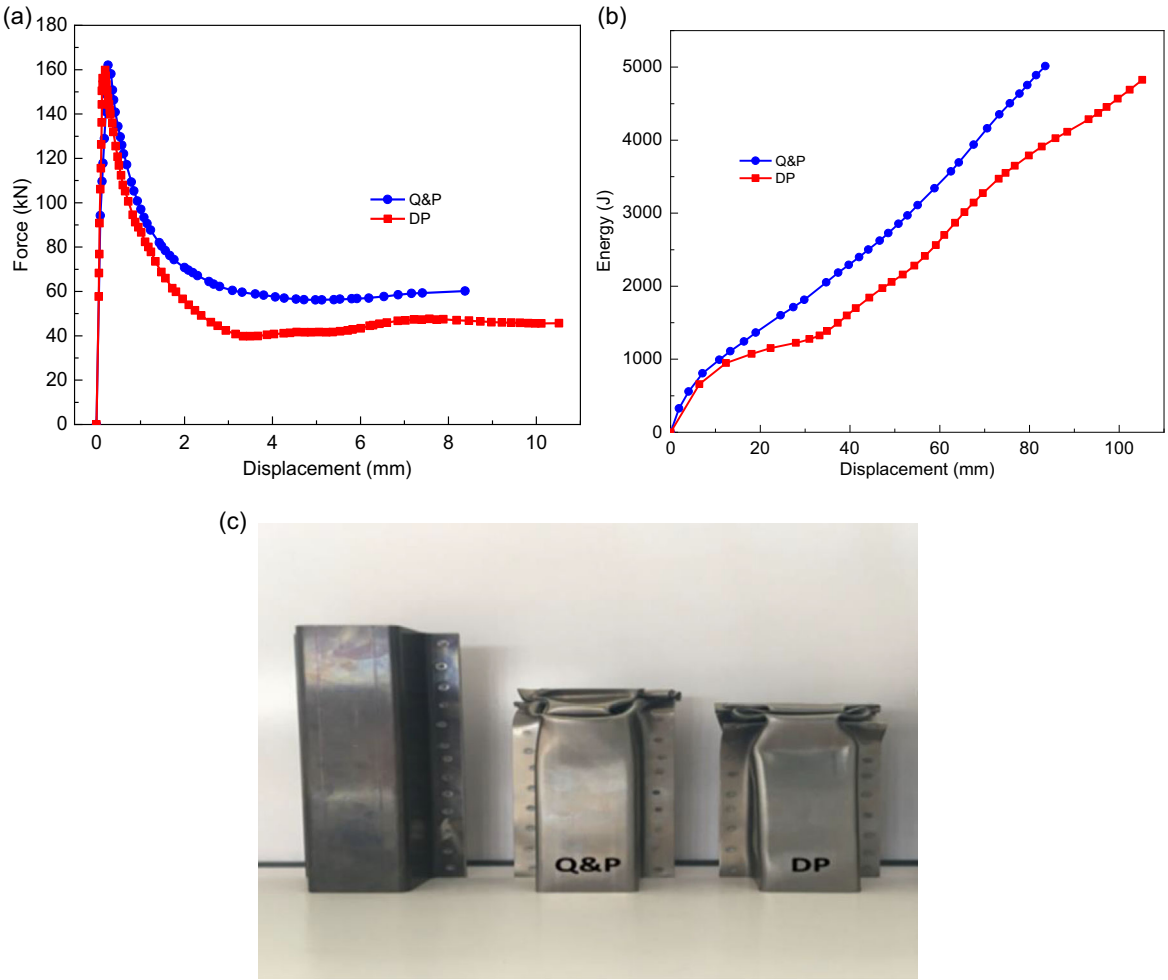

Figure 15. a) Average force–displacement curves and b) energy absorption–displacement curves for Q&P and DP 1030 steel during impact testing, and c) images of thin-walled structures made of both steels before and after testing. Reproduced with permission.[66] Copyright 2020, The Indian Institute of Metals, IIM.

© 2025 Wiley-VCH GmbH

15272648, 0, Downloaded from https://advanced.onlinelibrary.wiley.com/doi/10.1002/adem.202402016 by Technical University Delft, Wiley Online Library on [04/03/2025]. See the Terms and Conditions (https://onlinelibrary.wiley.com/terms-and-conditions) on Wiley Online Library for rules of use; OA articles are governed by the applicable Creative Commons License

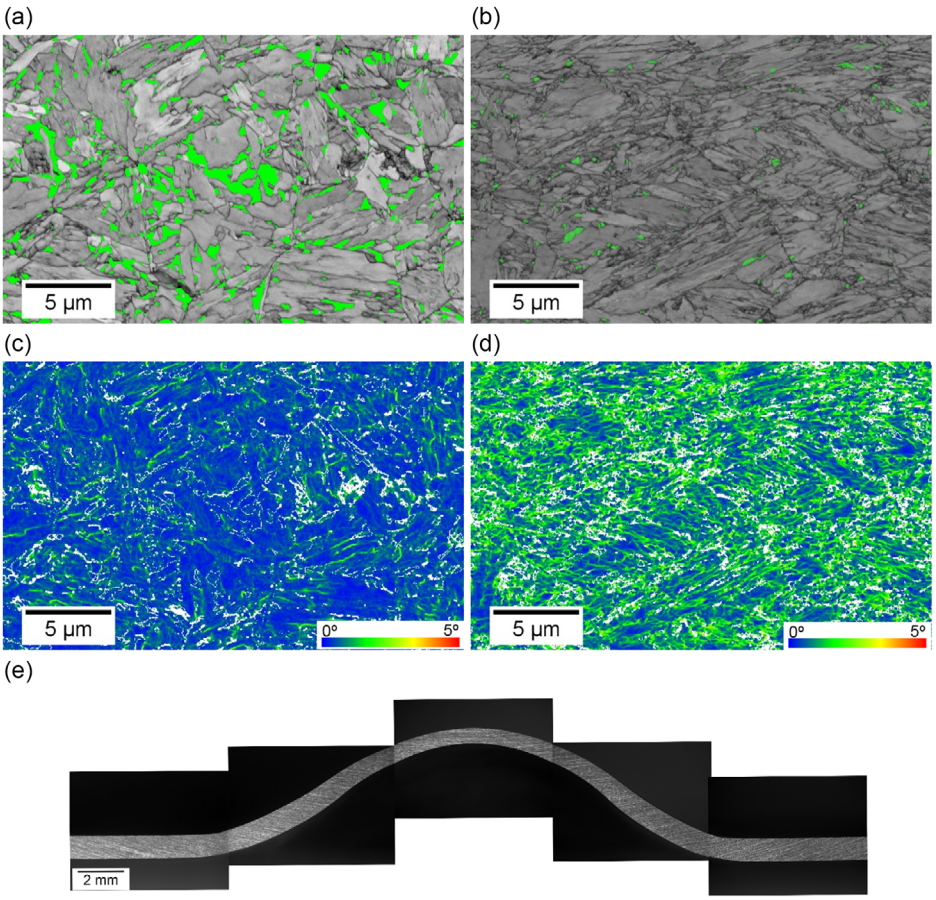

Figure 16. Band contrast map (with gray color) and RA phase map (with green color) of the tested specimens: a) as-received material and b) impacted with 60 J (a true strain of 28.6% was measured at the apex). c,d) Corresponding KAM maps (5°, 3rd) of (a) and (b), respectively. The volume fractions of RA detected via EBSD method in (a) and (b) are 9.6% and 1.2%, respectively. e) Section profile of the sample impacted with 90 J. Reproduced with permission.[25] Copyright 2018, Elsevier B.V.

observed during quasistatic punch testing at room temperature using the same impactor.

3.4. Comparison of the Impact Performance of the First-, Second-, and Third-Generation AHSS

The overview of the results presented above indicates a significant difference in the impact performance of the first-, second-, and third-generation AHSS. It is important to note that impact testing conditions and configurations can significantly influence the results, leading to contradictory conclusions due to the lack of standardized testing methods. Different hardening approaches, such as prestraining, can be employed to enhance the energy absorption capacity of AHSS. In the case of thin-walled structures, third-generation AHSS typically has higher mean force ratios than second-generation AHSS, while first-generation AHSS exhibits the highest peak/mean force ratios (see Figure 8, 11, 14, and 15). From a passenger safety perspective during crash accidents, AHSS with low peak/mean force ratios is more suitable for automotive applications.

Table 2 summarizes the mechanical properties and impact resistance data (the maximum energy absorbed before fracture) of AHSS sheets from three different generations, all subjected to drop weight impact testing under the same conditions (including sample dimensions, impactor, temperature, fastening method, and lubrication protocols). The 304 SS exhibits the best performance, with a maximum absorbed energy of 130 J, followed by the Q&P steel with 110 J and the DP1180 AHSS with 90 J.[25,44,67] Selected force–displacement curves from these tests are compared in **Figure 17**. Impact testing of these AHSS with 110 J energy (Table 2) demonstrates that the DP1180 steel has the most pronounced adiabatic heating effect, followed by the Q&P steel and the 304 SS. The temperature increase (ΔT) in the DP1180 steel reaches up to 202 °C, while for 304 SS and Q&P steel, the ΔT values are 121 and 164 °C, respectively.

Table 2 shows that the DP1180 steel accumulates a higher plastic strain (81.1%) than the 304 SS (45.5%) or Q&P steel (42.2%) under the same impact energy. This can be related to the low-strain hardening ability of the DP1180 steel, which causes macro-localization of plastic deformation at the top of the dome (Figure 16e). A possible explanation for the relatively low impact performance of the DP1180 steel could be its sole

 © 2025 Wiley-VCH GmbH

15272648, 0, Downloaded from https://advanced.onlinelibrary.wiley.com/doi/10.1002/adem.202402016 by Technical University Delft, Wiley Online Library on [04/03/2025]. See the Terms and Conditions (https://onlinelibrary.wiley.com/terms-and-conditions) on Wiley Online Library for rules of use; OA articles are governed by the applicable Creative Commons License

Table 2. Comparison of mechanical properties and impact performance of AHSS from three different generations subjected to drop weight impact testing under the same conditions.

Gen.	Steel	$\sigma_{0.2}$ [MPa]	σ_{UTS} [MPa]	TE [%]	n	Impact resistance [J]	Plastic strain accumulated at the top of the dome impacted with 90 J [%]	Temperature increase upon 90 J impact [°C]	Deformation mechanisms	References
1	DP1180	1062	1244	8.2	0.10	90	81.1	202	Dislocation glide	[44]
2	304 SS	345	826	97.9	0.52	130	45.5	121	Dislocation glide, twinning, phase transformation	[67]
3	Q&P	821	1267	27.5	0.19	110	42.2	164	Dislocation glide, phase transformation	[25]

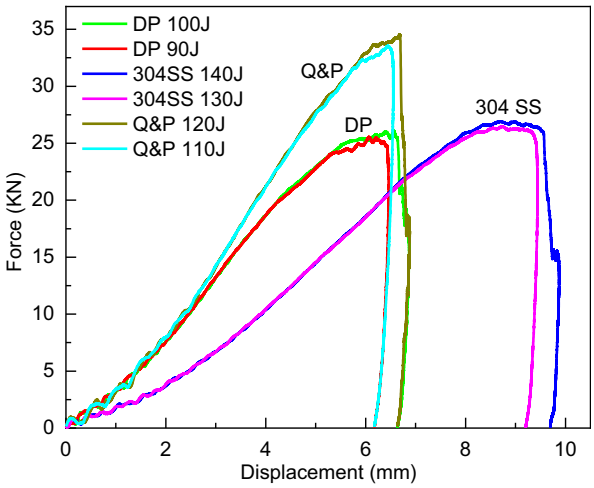

Figure 17. Force–displacement curves for DP1180, 304 SS, and Q&P steels during drop weight impact testing of sheet specimens.

reliance on the dislocation glide mechanism during high-strain-rate plastic deformation (Table 2). In contrast, the Q&P steel undergoes a RA–martensite phase transformation during high-strain-rate deformation, which enhances its strain hardening ability, increases ductility, and distributes plastic deformation over a larger volume. Both mechanisms improve the specimen's ability to absorb impact energy globally. In the case of 304 SS, the high-strain-rate deformation under impact is further "harmonized" by a higher contribution of austenite–martensite phase transformation into plastic deformation combined with twinning. Both effects lead to an even higher strain hardening ability of the material, increased energy absorption capacity, and reduced plastic strain accumulated at the top of the dome for the given impact energy. The latter is relevant to the measurement taken on the Q&P steel.

3.5. Effect of Welding on the Energy Absorption Capability of AHSS

Welding is the most widely used joining method in the automotive industry, and resistance spot welding (RSW) is the dominant welding method in the production of vehicle body structures due to its efficiency and cost-effectiveness. In RSW, the heat-affected zone (HAZ) is minimal because of the high electrical current density and short duration of the welding process, which minimizes the heat spread to the surrounding material. The HAZ is formed in the area of the material that is not melted during welding but is exposed to elevated temperatures, resulting in changes to the material's local microstructure and properties that can degrade the weld performance.[68] Spot welds with high load-bearing capacity and high-energy absorption capability are needed to maximize load transfer and energy dissipation during a collision event.

There is a body of experimental research examining the influence of RSW on the energy absorption capability of AHSS. RSW parameters were found to significantly affect the tensile properties, failure mode, and energy absorption of AHSS. In ref. [69], the energy absorption capability of DP600 tended to decrease with the reduction of weld nugget size, increased electrode indentation during expulsion, and the occurrence of single-sided instead of double-sided pull-out failure modes. The weld nugget size is the key factor controlling mechanical properties and energy absorption capability. Similar results were reported for DP800 and TRIP800 grades in ref. [70]. Comparison of different DP grades (DP600, DP780, and DP980) with varying levels of HAZ softening, as reported in ref. [71], revealed that HAZ softening could enhance the mechanical performance of welds. Specifically, it improved the load-bearing capacity and energy absorption capability by promoting pull-out failure mode even at smaller weld nugget size. Similar findings were observed in a study[72] focusing on AISI 304 AUST SS, where welding current influenced energy absorption. The energy absorption capability increased with weld nugget size in expulsion free samples but dropped significantly when expulsion occurred.

Despite these advancements in the field, the interplay between RSW parameters and the energy absorption capabilities of AHSS remains insufficiently explored. Future research should deepen insights into these relationships, enabling the development of optimized welding practices to meet the ever-increasing safety and performance demands of modern automotive design.

4. Approaches to Improve Impact Performance of AHSS

Several factors influence the impact energy absorption capacity of AHSS structures, including impact velocity, load orientation,

© 2025 Wiley-VCH GmbH

15272648, 0, Downloaded from https://advanced.onlinelibrary.wiley.com/doi/10.1002/adem.202402016 by Technical University Delft, Wiley Online Library on [04/03/2025]. See the Terms and Conditions (https://onlinelibrary.wiley.com/terms-and-conditions) on Wiley Online Library for rules of use; OA articles are governed by the applicable Creative Commons License

impactor geometry, structural design, and material properties. During an impact, only a small fraction of the energy is absorbed by elastic deformation. The vast majority of the energy is dissipated by plastic deformation of the material. Improving the impact performance and energy absorption capability of AHSS therefore requires high strength, adequate work hardening capacity, and ductility. It is a well-known fact that increasing mechanical strength often leads to a reduction in ductility, which is commonly referred to as the strength–ductility predicament. The fundamental strengthening mechanisms of metals can be simplified as the introduction of obstacles at different length scales to inhibit or block dislocation motion.[73] On the other hand, high ductility is achieved through mechanisms such as dislocation slip, TRIP, TWIP, microband-induced plasticity, or their combinations. Recently, numerous ultra-high strength steels have been developed using these strategies.[74–76] However, their impact performance remains uncertain, as impact involves complex deformation processes that are not directly correlated with strength and tensile ductility, as discussed in Section 3.

The impact/collision of vehicle components involves mixed dynamic deformation processes, characterized by multiaxial stress states that vary throughout the material's volume. To ensure passenger safety, these processes must effectively absorb impact energy. To meet such requirements, the materials used for safety parts (usually steels) must have both high strength with good formability under dynamic loading conditions. This is particularly true for the majority of the AHSS discussed in Section 3. Over the past few decades, extensive research efforts have been dedicated to developing novel high and ultra-high strength steel grades. These studies have explored various strategies to enhance the impact performance of steel, which are briefly summarized later.

4.1. Ultrafine Austenite Grains with TWIP Effect

Typically, conventional TWIP steels have a coarse-grained microstructure with a grain size of tens of micrometers, resulting in a relatively low yield strength (200–500 MPa). However, higher ultimate tensile strength values (≈1000 MPa) are frequently achieved after significant elongation (≈60%).[77,78]

It is evident that in order to absorb a significant amount of energy, a large amount of deformation must occur. While absorbing large amounts of energy requires substantial deformation, this is impractical for automotive energy absorption components due to the limited deformation allowed during crash events. For instance, during impact testing on thin-walled structures, unstrengthened TWIP steels require a longer impact displacement than strengthened TWIP steels to consume the same amount of impact energy, as demonstrated in Figure 14. Therefore, to meet the requirements of the automotive industry, traditional coarse-grained TWIP steels have to be strengthened before use. In addition to work hardening/prestraining, grain refinement is an effective method to improve strength. Grain refinement has been shown to benefit most steels,[79,80] and TWIP steels are no exception. Studies widely report that grain refinement enhances strength in TWIP steels. For example, in ref. [81], multiple cold rolling and annealing processes were employed to produce ultrafine austenite grains with an average

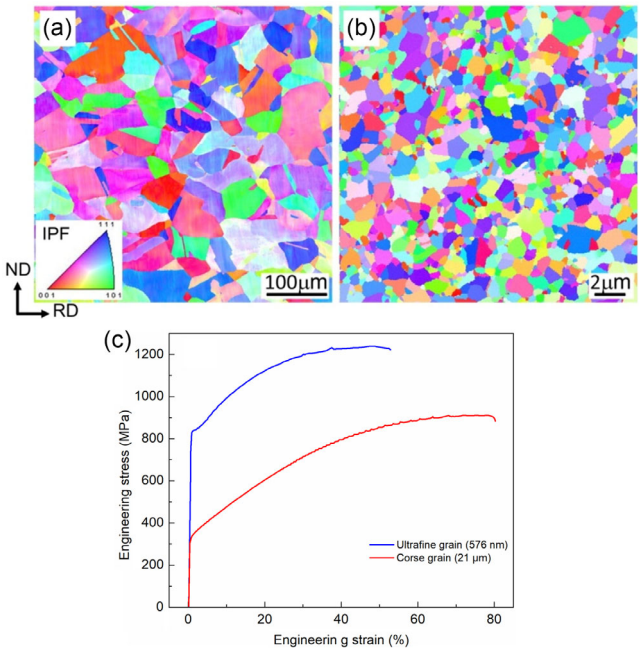

Figure 18. Normal direction inverse pole figure map of a) coarse and b) ultrafine grained TWIP steels. c) Engineering stress–strain curves of coarse and ultrafine grained TWIP steels. Reproduced with permission.[81] Copyright 2017, Elsevier Inc.

size of 576 nm. The microstructures and engineering stress–strain curves of coarse and ultrafine-grained TWIP steels are compared in **Figure 18**. It is clear that the grain refinement doubled the yield strength, while maintaining excellent strain hardening ability and tensile elongation (see Figure 18c). Improved impact performance in fine-grained TWIP steel can be expected based on its uniaxial tensile properties, although no impact testing has been reported on this material yet. Furthermore, grain refinement has significantly mitigated the hydrogen embrittlement issue, a persistent challenge in TWIP steels, offering further potential for practical application.[82]

4.2. Micro- and Macro-Lamellar Structure

Deformation and partitioning (D&P) steels have lamellar martensite–austenite duplex microstructure, which provides a yield strength of 2 GPa or even higher.[75,76] Their typical lamellar microstructure is shown in **Figure 19**a. In D&P steels, the density of dislocations in the martensite is at least one order of magnitude higher than that in common MART steels, contributing to their ultra-high strength.[75,76] These steels achieve a notable total elongation of 21.6%[76] (Figure 19b), primarily through the combination of dislocation slip and TRIP effect. The representative engineering stress–strain curves of D&P steels are shown in Figure 19b. Despite their impressive tensile properties, the impact performance of D&P steels may be inferior due to various reasons: 1) the abrupt yielding effect in tension may induce very high peak forces during impact loading of thin-walled structures made of this steel; 2) the material exhibits low strain hardening ability; and 3) the lamellar microstructure may be unfavorable for

© 2025 Wiley-VCH GmbH

15272648, 0, Downloaded from https://advanced.onlinelibrary.wiley.com/doi/10.1002/adem.202402016 by Technical University Delft, Wiley Online Library on [04/03/2025]. See the Terms and Conditions (https://onlinelibrary.wiley.com/terms-and-conditions) on Wiley Online Library for rules of use; OA articles are governed by the applicable Creative Commons License

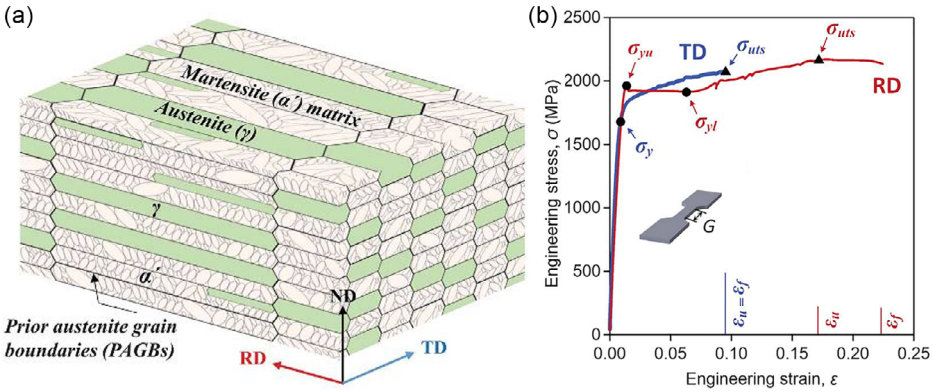

Figure 19. a) Schematic 3D model illustrates the lamellar martensite–austenite heterogeneous microstructure of the D&P steel; b) engineering stress–strain curves in RD and TD. Reproduced with permission.[76] Copyright 2020, The American Association for the Advancement of Science.

accommodating shearing and bending deformation, which are prevalent in impact events. Anisotropy in total elongation observed during tensile testing, as shown in Figure 19b, suggests that cracks may initiate earlier in certain directions, further complicating their use in impact scenarios. Furthermore, the high carbon content (0.4–0.5 wt%) used in D&P steels may handicap their application in automobiles due to low weldability. Consequently, further research is necessary to address these limitations and enhance the applicability of D&P steels in automotive components.

In addition, a "lamellar" structure can also be engineered on a macroscale by modifying the local mechanical properties of thin-walled structures. This modification improves their impact performance by increasing the mean impact force. For instance, TWIP1000 can be treated with laser heat treatment to create this structure by periodically and intermittently heating specific areas to form cyclic soft–hard zones, as reported in ref. [61]. The laser-treated zones have higher strength than non-treated zones, enabling them to withstand higher loads during impact. An image of laser-treated specimens and the corresponding impact testing results are shown in **Figure** 14 and **20**, respectively. Under identical impact energy, the laser-treated samples required a shorter displacement to absorb the energy compared to recrystallized samples, as demonstrated in Figure 14c. This indicates a significant enhancement in impact performance. It should be noted that such a macro-lamellar structure can also be created through other methods, such as local mechanical treatment. Further research is needed to optimize the distribution, arrangement, shape, size, and other characteristics of the soft and hard zones to maximize their performance benefits.

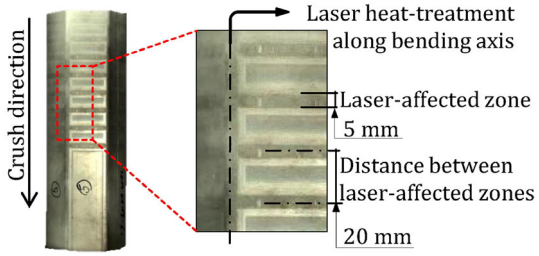

Figure 20. Laser local heat-treated thin-walled structure. Reproduced with permission.[61] Copyright 2016, Elsevier Ltd.

4.3. Precipitates

Precipitates have been widely used as the main or secondary strengthening mechanism in many high strength steels (HSS) as they impede dislocation movement.[83] Two representative HSS designed based on precipitation hardening are: 1) Nanohiten steels, which are based on the low-alloy Fe–C–Mn–Si system. These steels consist of a ferrite matrix and nano-sized carbides formed by adding a small amount of titanium and/or molybdenum (<0.5 wt%).[84] 2) Modified maraging steels is another category, which has a high nickel (≈18 wt%) and molybdenum (≈4 wt%) content.[84,85] The latter has a martensite matrix with a high density of nanoprecipitates embedded in it.[85] Nanohiten steels are characterized by much lower cost due to the absence of costly alloying elements. In general, Nanohiten steels exhibit superior ductility compared to maraging steels, although they have relatively lower strength, as shown in **Figure 21**. The difference in properties between Nanohiten and maraging steels can be attributed to their different matrices. Nanohiten steels have a ferrite matrix, while maraging steels have a martensite matrix. Additionally, Nanohiten steels have demonstrated excellent formability, as evidenced by their enhanced hole expansion ratio,[84] making them advantageous for automotive applications. In contrast, the ductility of modified maraging steels is limited, typically around 8%, which may result in premature cracking during impact events. Therefore, it is reasonable to conclude that Nanohiten steels are a more advantageous choice than modified maraging steels for applications requiring impact energy absorption, considering both impact performance and manufacturing costs.

Furthermore, the application of precipitate hardening has enabled conventional HSS to achieve remarkable mechanical properties. A representative example is conventional HSLA steels, which typically exhibit a UTS below 800 MPa.[35,86,87] However, their UTS can exceed 800 MPa by the addition of alloying elements, such as Cu, Ni, Mo, Nb, and Ti.[88–96] The matrix of these strengthened HSLA steels is typically tempered martensite with embedded precipitates. The size and distribution of these

© 2025 Wiley-VCH GmbH

15272648, 0, Downloaded from https://advanced.onlinelibrary.wiley.com/doi/10.1002/adem.202402016 by Technical University Delft, Wiley Online Library on [04/03/2025]. See the Terms and Conditions (https://onlinelibrary.wiley.com/terms-and-conditions) on Wiley Online Library for rules of use; OA articles are governed by the applicable Creative Commons License

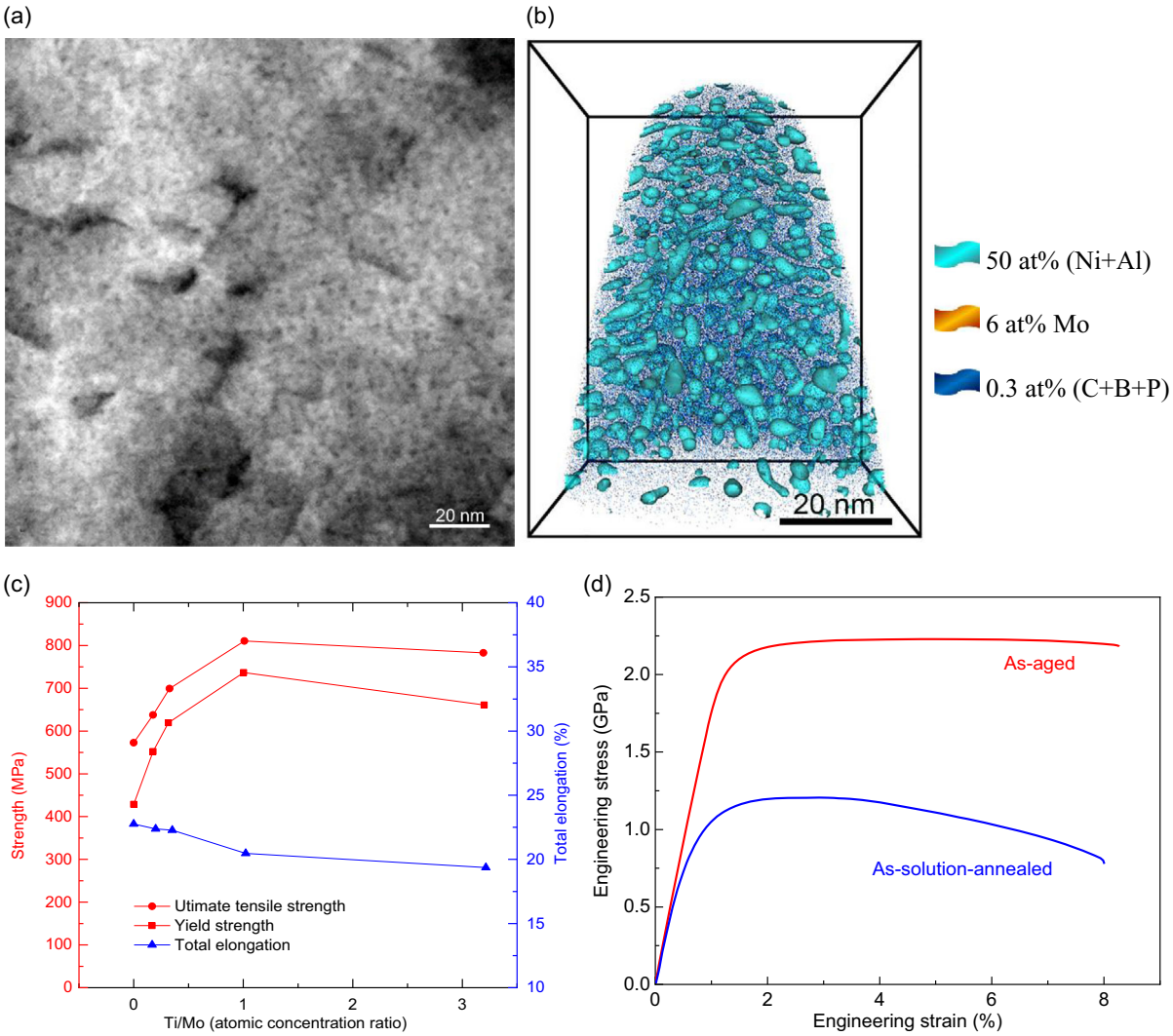

Figure 21. a) Transmission electron microscopy (TEM) image and b) atom map of aged maraging steel.[85] c) Tensile mechanical properties of Nanohiten steels.[84] d) Engineering stress–strain curves of novel maraging steels.[85] In (b), precipitates are highlighted by isoconcentration surface encompassing regions containing more than 50 at% of Al and Ni combined. (a,b,d) Reproduced with permission.[85] Copyright 2017, Macmillan Publishers Limited, part of Springer Nature.

precipitates significantly influence the mechanical properties of HSLA steels, which can be regulated through tempering temperature and time. For instance, an experimental study demonstrated that by adjusting heat treatment parameters, the UTS and YS can be altered in a range of 887–1391 and 793–1332 MPa, respectively. Similar reports can be found in refs. [89,93,97,98]. This broad range of mechanical properties is advantageous for meeting diverse application requirements. Moreover, studies have demonstrated that modified HSLA steels exhibit excellent toughness during Charpy impact testing, even at low temperatures. For instance, an impact toughness of 237 J cm^{-2} was reported at –40 °C in ref. [90] and 204 J cm^{-2} at the same temperature in ref. [89]. These findings suggest that modified HSLA steels have the potential for automobile impact applications. However, many of these grades contain relatively high contents of expensive alloying elements, such as Ni, Mo, and V,[88–90] making it necessary to conduct further research on alloy design to reduce the reliance on these costly elements.

4.4. Modification of Martensite, RA, and/or Precipitates

Significant progress has been made in the development of HSS through the modification of conventional microstructures based on martensite, RA, and (nano)precipitates. In summary, martensite and precipitates contribute to high strength, while RA promotes ductility. The related TRIP effect also enhances the strain hardening ability. For cost considerations, steels based on the Fe–C–Mn–Si system with lean alloying elements are commonly used. These steels employ various strengthening mechanisms such as grain refinement, precipitates, dislocations, and solid solution to control their strength. Two representative examples of these steels are Q&P steel and

© 2025 Wiley-VCH GmbH

15272648, 0, Downloaded from https://advanced.onlinelibrary.wiley.com/doi/10.1002/adem.202402016 by Technical University Delft, Wiley Online Library on [04/03/2025]. See the Terms and Conditions (https://onlinelibrary.wiley.com/terms-and-conditions) on Wiley Online Library for rules of use; OA articles are governed by the applicable Creative Commons License

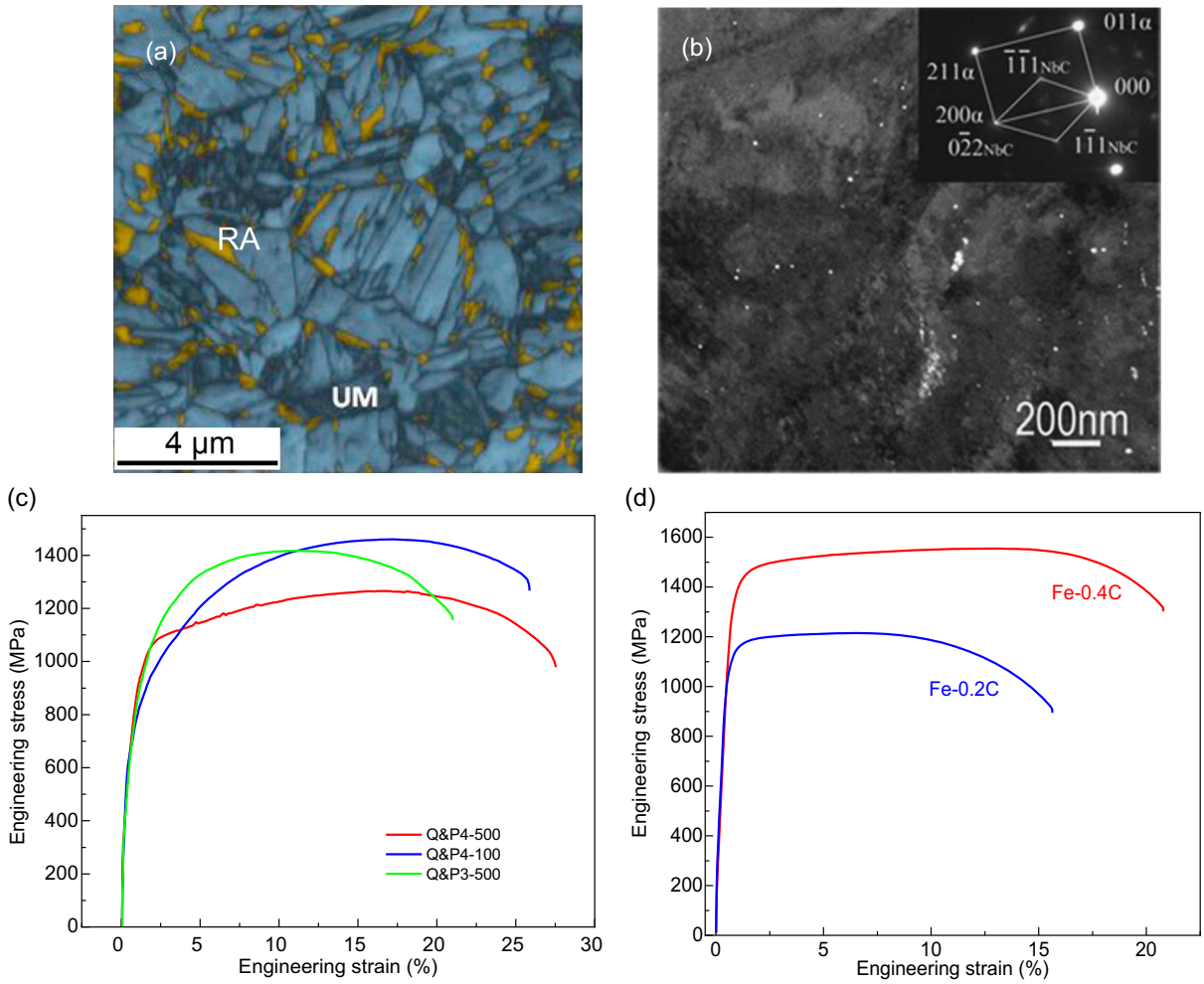

Figure 22. Typical microstructures of a) Q&P[101] and b) Q–P–T[99] steels: (a) EBSD phase map overlaid with image quality map, where RA is in yellow and martensite in blue. (b) TEM dark-field image showing nanoprecipitates. Tensile engineering stress–engineering strain curves of c) Q&P[101] and d) Q–P–T steels.[99] UM: untempered martensite. (a,c) Reproduced with permission.[99] Copyright 2014, Elsevier B.V; (b,d) Reproduced with permission.[101] Copyright 2015, Elsevier B.V.

quenching–partitioning–tempering (Q–P–T) steel.[99] The key differences between these two steels are that 1) Q&P steels do not involve tempering as the final step during its processing and 2) Q&P steels typically have no precipitates. Typical microstructures of these two steels are presented in **Figure 22**a,b, respectively. The representative engineering stress–strain curves of Q&P and Q–P–T steels are shown in Figure 22c,d, respectively, indicating high strength and good ductility. Q&P steels generally exhibit higher ductility and better strain hardening ability but lower strength compared to Q–P–T steels, due to differences in RA fractions and precipitates. As a result, Q&P steels are expected to have better impact resistance. However, to meet the energy absorption requirements of automotive applications, the formability of Q–P–T steels must be further improved.

5. Summary and Outlook

We have reviewed the impact performance of three generations of AHSS using impact tests on thin-walled structures and plate specimens. When evaluating thin-walled structures, second-generation AHSS exhibit lower energy absorption capacity compared to first- and third-generation AHSS. This difference can be attributed to the lower yield strength of second-generation AHSS. However, the lower yield strength also results in a more stable impact response for second-generation AHSS, which is beneficial for occupant safety. The stability of the impact response has received limited research attention and deserves further investigation. Tremendous research has shown that increasing yield strength enhances the ability of thin-walled structures to absorb high impact energy. However, this often leads to significantly higher peak force/mean force ratios, which can be detrimental to passenger safety in automotive applications. Further investigations are required to "flatten" the force–displacement curves of AHSS with high yield strengths. Additionally, future studies should account for both weight and thickness when evaluating the impact energy absorption of AHSS.

In contrast, when sheet samples are evaluated, the second-generation AHSS shows the best impact resistance due to its

© 2025 Wiley-VCH GmbH

15272648, 0, Downloaded from https://advanced.onlinelibrary.wiley.com/doi/10.1002/adem.202402016 by Technical University Delft, Wiley Online Library on [04/03/2025]. See the Terms and Conditions (https://onlinelibrary.wiley.com/terms-and-conditions) on Wiley Online Library for rules of use; OA articles are governed by the applicable Creative Commons License

15272648, 0, Downloaded from https://advanced.onlinelibrary.wiley.com/doi/10.1002/adem.202402016 by Technical University Delft, Wiley Online Library on [04/03/2025]. See the Terms and Conditions (https://onlinelibrary.wiley.com/terms-and-conditions) on Wiley Online Library for rules of use; OA articles are governed by the applicable Creative Commons License

excellent work hardening ability and formability. The third-generation AHSS follows closely in terms of impact performance, while the first-generation AHSS exhibits significantly lower impact resistance. However, third-generation AHSS are particularly attractive for automotive components due to their lower cost and exceptional mechanical properties, which are critical for meeting high energy absorption requirements.

In addition, an overview of several potential approaches to improve the impact performance of AHSS is provided, including 1) ultrafine austenite with TWIP effect; 2) micro- and macro-lamellar structures; 3) precipitates; and 4) modifications of RA, and/or precipitates. While these strategies have achieved remarkable tensile mechanical properties, not all of them may be suitable for automotive applications involving energy absorption.

The current study has provided a basis for understanding the impact performance of different generations of AHSS in thin-walled structures and sheet specimens. However, the impact performance of these materials has not been extensively investigated, and there is a lack of a standardized evaluation framework. There is substantial scope for further research in this area, and the following areas of investigation are strongly recommended to enhance our understanding and improve the impact performance of AHSS. 1) There is currently no test standard specifically designed to evaluate the impact behavior of thin-walled structures and sheets of AHSS. Developing standardized testing setups and protocols would help provide a more accurate representation of the impact properties of AHSS. This would facilitate comparison and collaboration between different research teams. 2) For sheet metal, the impact deformation process involves various loading modes, such as tension, bending, biaxial stretching, and shearing. Any weakness in the material's response to these loads can lead to premature cracking and undermine its ability to absorb impact energy effectively. It is therefore essential to identify the weak links in the mechanical properties. 3) Deformation mechanisms are closely related to the microstructure of the material, the applied stress mode, and strain rate. Using numerical simulations, researchers can accurately describe the stress states at different stages of deformation. Synergistic investigations combining both experimental tests and simulations are required to fully understand the deformation behavior of AHSS under impact conditions. 4) Based on existing research results, different strategies should be adopted to improve the impact performance of thin-walled structures and sheet materials. For thin-walled structures, attention should focus on increasing the mean impact force, which is mainly influenced by the steady collapse stage. Moreover, reducing the high peak force is crucial, as it results in high accelerations at the onset of a collision, which could be detrimental to passenger safety. 5) In the case of sheet metal components, strength, ductility, and work hardening properties are critical to improving their impact performance. In addition, it is important to optimize the material resistance to shear and biaxial loading conditions, as these factors significantly contribute to the overall impact energy absorption. 6) The effect of crystallographic texture on impact performance of AHSS remains unexplored and is worthy of investigation. In rolled steel sheets, a strong crystallographic texture can result in an enhanced deformation capacity along the rolling direction (RD), but reduce it in the perpendicular direction. The impact deformation process is inherently multidirectional, and due to the presence of texture, premature cracking is more likely to occur in the transverse direction (TD), preventing the material's ability to absorb impact energy effectively. Texture control may, therefore, be used to improve impact performance of AHSS. 7) Key parameters, such as weld nugget size and HAZ softening, significantly influence the mechanical properties and energy absorption capabilities of resistance spot welds. Optimizing these factors can enhance load-bearing capacity, energy absorption, and failure modes during collisions. Continued research on the interplay of welding parameters and energy absorption will be essential to meet the evolving safety and performance demands of automotive design.

Acknowledgements

P.X. acknowledges gratefully the financial support from the China Scholarship Council (no. 201606890031, Beijing, China). The authors acknowledge gratefully the funding from the Research Fund for Coal and Steel (RFCS) under Grant Agreement 709755 (OptiQPAP project).

Conflict of Interest

The authors declare no conflict of interest.

Author Contributions

Peikang Xia: conceptualization (equal); investigation (equal); methodology (equal); validation (equal); visualization (lead); writing—original draft (lead). **Ilchat Sabirov**: conceptualization (equal); funding acquisition (lead); investigation (equal); methodology (equal); project administration (equal); supervision (lead); validation (equal); writing—review & editing (equal). **Roumen Petrov**: conceptualization (equal); investigation (equal); methodology (equal); project administration (equal); validation (equal); writing—review & editing (equal). **Patricia Verleysen**: conceptualization (equal); investigation (equal); methodology (equal); project administration (equal); validation (equal); writing—review & editing (equal).

Keywords

advanced high strength steels, energy absorption, impact performance, microstructure, thin-walled structures

Received: August 28, 2024
Revised: December 22, 2024
Published online:

[1] J.-H. Schmitt, T. Iung, *C. R. Phys.* **2018**, *19*, 641.
[2] J. Galán, L. Samek, P. Verleysen, K. Verbeken, Y. Houbaert, *Rev. Metal.* **2012**, *48*, 118.
[3] J. Zhao, Z. Jiang, *Prog. Mater. Sci.* **2018**, *94*, 174.
[4] K. Radwanski, R. Kuziak, R. Rozmus, *Arch. Civ. Mech. Eng.* **2019**, *19*, 453.
[5] S. Li, R. Zhu, I. Karaman, R. Arróyave, *Acta Mater.* **2012**, *60*, 6120.
[6] R. d. M. C. Lima, F. Tereza dos Santos Fernandes Tolomelli, A. J. Clarke, K. D. Clarke, J. C. Spadotto, F. C. R. Assunção, *J. Mater. Res. Technol.* **2022**, *17*, 184.
[7] G. Krauss, *Mater. Sci. Eng., A* **1999**, *273–275*, 40.

 © 2025 Wiley-VCH GmbH

[8] O. Bouaziz, S. Allain, C. P. Scott, P. Cugy, D. Barbier, *Curr. Opin. Solid State Mater. Sci.* **2011**, *15*, 141.
[9] D. V. Edmonds, K. He, F. C. Rizzo, B. C. De Cooman, D. K. Matlock, J. G. Speer, *Mater. Sci. Eng., A* **2006**, *438–440*, 25.
[10] P. S. R. Narayana, R. V. Prakash, S. Gunti, K. Raghu, *ASME Open J. Eng.* **2022**, *1*, 011050.
[11] B. Hance, *SAE Int. J. Mater. Manuf.* **2018**, *11*, 505.
[12] B. Yan, D. Urban, *Characterization of Fatigue and Crash Performance of New Generation High Strength Steels for Automotive Applications*, Idaho Operations Office, American Iron and Steel Institute/U.S. Department of Energy Technology Roadmap Program, Pittsburgh, PA **2003**, https://doi.org/10.2172/812199.
[13] G. Chen, M. F. Shi, T. Tyan, *SAE Int. J. Mater. Manuf.* **2012**, *5*, 304.
[14] D. Frómeta, A. Lara, S. Molas, D. Casellas, J. Rehrl, C. Suppan, P. Larour, J. Calvo, *Eng. Fract. Mech.* **2019**, *205*, 319.
[15] D. Frómeta, S. Parareda, A. Lara, L. Grifé, I. Tarhouni, D. Casellas, *IOP Conf. Ser.: Mater. Sci. Eng.* **2021**, *1157*, 012094.
[16] W. Abramowicz, *Int. J. Impact Eng.* **1983**, *1*, 309.
[17] Q. Q. Li, E. Li, T. Chen, L. Wu, G. Q. Wang, Z. C. He, *Thin-Walled Struct.* **2021**, *162*, 107588.
[18] M. D. White, N. Jones, *Int. J. Mech. Sci.* **1999**, *41*, 179.
[19] V. Tarigopula, M. Langseth, O. S. Hopperstad, A. H. Clausen, *Int. J. Impact Eng.* **2006**, *32*, 847.
[20] F. Xu, G. Sun, G. Li, Q. Li, *Thin-Walled Struct.* **2014**, *74*, 12.
[21] F. Tarlochan, F. Samer, A. M. S. Hamouda, S. Ramesh, K. Khalid, *Thin-Walled Struct.* **2013**, *71*, 7.
[22] Z. Li, S. Rakheja, W.-B. Shangguan, *Thin-Walled Struct.* **2019**, *145*, 106376.
[23] G. Gruben, M. Langseth, E. Fagerholt, O. S. Hopperstad, *Int. J. Impact Eng.* **2016**, *88*, 153.
[24] B. Liu, R. Villavicencio, C. Guedes Soares, *Mech. Sci.* **2014**, *80*, 1.
[25] P. Xia, I. Sabirov, J. Molina-Aldareguia, P. Verleysen, R. Petrov, *Mater. Sci. Eng., A* **2018**, *737*, 18.
[26] J. A. Rodríguez-Martínez, A. Rusinek, P. Chevrier, R. Bernier, A. Arias, *Int. J. Impact Eng.* **2010**, *37*, 828.
[27] K. Sato, T. Inazumi, A. Yoshitake, S.-D. Liu, *Int. J. Impact Eng.* **2013**, *54*, 1.
[28] A. G. Hanssen, T. Auestad, T. Tryland, M. Langseth, *Int. J. Crashworthiness* **2003**, *8*, 385.
[29] B. P. DiPaolo, P. J. M. Monteiro, R. Gronsky, *Int. J. Solids Struct.* **2004**, *41*, 3707.
[30] W. Abramowicz, N. Jones, *Int. J. Impact Eng.* **1984**, *2*, 179.
[31] R. Nightingale, *Shock Vib.* **1999**, *6*, 111.
[32] R. J. Hayduk, T. Wierzbicki, *Comput. Struct.* **1984**, *18*, 447.
[33] T. Wierzbicki, W. Abramowicz, *J. Appl. Mech.* **1983**, *50*, 727.
[34] W. Abramowicz, T. Wierzbicki, *J. Appl. Mech.* **1989**, *56*, 113.
[35] D. Schaeffler, M. Kimchi, Advanced High Strength Steels Applications Guidelines V7.0, WorldAutoSteel **2021**, https://ahssinsights.org/blog/welcome-to-the-all-new-ahss-application-guidelines/ (accessed: November 2023).
[36] N. Abedrabbo, R. Mayer, A. Thompson, C. Salisbury, M. Worswick, I. van Riemsdijk, *Int. J. Impact Eng.* **2009**, *36*, 1044.
[37] J. R. Fekete, A. M. Stibich, M. F. Shi, SAE Technical Paper 2001-01-3101, **2001**, https://doi.org/10.4271/2001-01-3101.
[38] N. Peixinho, N. Jones, A. Pinho, *J. Phys. IV* **2003**, *110*, 717.
[39] I. Hajiannia, M. Shamanian, M. Atapour, E. Ghassemali, N. Saeidi, *Trans. Indian Inst. Met.* **2018**, *71*, 1363.
[40] C. Lesch, N. Kwiaton, F. B. Klose, *Steel Res. Int.* **2017**, *88*, 1700210.
[41] G. Sun, M. Deng, G. Zheng, Q. Li, *Thin-Walled Struct.* **2019**, *138*, 458.
[42] X. Song, G. Sun, Q. Li, *Thin-Walled Struct.* **2016**, *109*, 132.
[43] J. K. Holmen, O. S. Hopperstad, T. Børvik, *Int. J. Impact Eng.* **2015**, *78*, 161.
[44] P. Xia, M. Sanchez Palomar, I. Sabirov, *Mater. Sci. Eng., A* **2020**, *785*, 139382.
[45] X. M. Chen, M. F. Shi, G. Chen, M. Kamura, K. Watanabe, Y. Omiya, SAE Technical Paper 2005-01-0354 **2005**, https://doi.org/10.4271/2005-01-0354.
[46] T. J. Reddy, Y. V. D. Rao, V. Narayanamurthy, *Int. J. Crashworthiness* **2017**, *23*, 57.
[47] E. Pereloma, A. Gazder, I. Timokhina, *Encyclopedia of Iron Steel their Alloys Online Version*, CRC Press, Boca Raton, FL **2016**.
[48] J. A. Rodríguez-Martínez, R. Pesci, A. Rusinek, A. Arias, R. Zaera, D. A. Pedroche, *Int. J. Solids Struct.* **2010**, *47*, 1268.
[49] I. D. Choi, D. M. Bruce, S. J. Kim, C. G. Lee, S. H. Park, D. K. Matlock, J. G. Speer, *ISIJ Int.* **2002**, *42*, 1483.
[50] J. Van Slycken, P. Verleysen, J. Degrieck, L. Samek, B. C. de Cooman, *Metall. Mater. Trans. A* **2006**, *37*, 1527.
[51] F. Vercruysse, C. Celada-Casero, B. M. Linke, P. Verleysen, R. H. Petrov, *Metals* **2020**, *10*, 509.
[52] L. Durrenberger, X. Lemoine, A. Molinari, *J. Mater. Process. Technol.* **2011**, *211*, 1937.
[53] N. Ormsuptave, V. Uthaisangsuk, *Steel Res. Int.* **2016**, *88*, 1600150.
[54] Z. C. Wang, S. J. Kim, C. G. Lee, T. H. Lee, *J. Mater. Process. Technol.* **2004**, *151*, 141.
[55] E. Ratte, S. Leonhardt, W. Bleck, M. Franzen, P. Urban, *Steel Res. Int.* **2006**, *77*, 692.
[56] L. L. Wei, G. H. Gao, J. Kim, R. D. K. Misra, C. G. Yang, X. J. Jin, *Mater. Sci. Eng., A* **2022**, *838*, 142829.
[57] K. Li, V. S. Y. Injeti, R. D. K. Misra, Z. H. Cai, H. Ding, *Mater. Sci. Eng., A* **2018**, *711*, 515.
[58] D. Cornette, P. Cugy, A. Hildenbrand, M. Bouzekri, G. Lovato (Arcelor), *Rev. Métall.* **2005**, *102*, 905.
[59] M. Daamen, O. Güvenç, M. Bambach, G. Hirt, *CIRP Ann.* **2014**, *63*, 265.
[60] O. Güvenç, F. Roters, T. Hickel, M. Bambach, *JOM* **2014**, *67*, 120.
[61] M. Bambach, L. Conrads, M. Daamen, O. Güvenç, G. Hirt, *Mater. Des.* **2016**, *110*, 157.
[62] Y. Liu, *Int. J. Crashworthiness* **2008**, *13*, 543.
[63] B. P. DiPaolo, J. G. Tom, *Int. J. Solids Struct.* **2006**, *43*, 7752.
[64] J. A. Rodríguez-Martínez, A. Rusinek, R. Pesci, *Thin-Walled Struct.* **2010**, *48*, 966.
[65] J. A. Rodríguez-Martínez, A. Rusinek, R. Pesci, R. Zaera, *Int. J. Solids Struct.* **2013**, *50*, 339.
[66] D. Zhou, M. Xu, Z. Mi, *Trans. Indian Inst. Met.* **2020**, *73*, 1999.
[67] P. Xia, F. J. Canillas Rodríguez, I. Sabirov, *Mater. Sci. Eng., A* **2020**, *793*, 139829.
[68] M. Pouranvari, S. P. H. Marashi, *Sci. Technol. Weld. Joining* **2010**, *15*, 149.
[69] H. L. Jaber, M. Pouranvari, R. K. Salim, F. A. Hashim, S. P. H. Marashi, *Ironmaking Steelmaking* **2016**, *44*, 699.
[70] X. Sun, E. V. Stephens, M. A. Khaleel, *Eng. Fail. Anal.* **2008**, *15*, 356.
[71] M. Pouranvari, S. P. H. Marashi, D. S. Safanama, *Mater. Sci. Eng., A* **2011**, *528*, 8344.
[72] M. Pouranvari, E. Ranjbarnodeh, *Res. J. Appl. Sci., Eng. Technol.* **2012**, *4*, 2911.
[73] K. Lu, L. Lu, S. Suresh, *Science* **2009**, *324*, 349.
[74] S.-H. Kim, H. Kim, N. J. Kim, *Nature* **2015**, *518*, 77.
[75] B. B. He, B. Hu, H. W. Yen, G. J. Cheng, Z. K. Wang, H. W. Luo, M. X. Huang, *Science* **2017**, *357*, 1029.
[76] L. Liu, Q. Yu, Z. Wang, J. Ell, M. X. Huang, R. O. Ritchie, *Science* **2020**, *368*, 1347.
[77] O. Grässel, L. Krüger, G. Frommeyer, L. W. Meyer, *Int. J. Plast.* **2000**, *16*, 1391.

© 2025 Wiley-VCH GmbH

15272648, 0, Downloaded from https://advanced.onlinelibrary.wiley.com/doi/10.1002/adem.202402016 by Technical University Delft, Wiley Online Library on [04/03/2025]. See the Terms and Conditions (https://onlinelibrary.wiley.com/terms-and-conditions) on Wiley Online Library for rules of use; OA articles are governed by the applicable Creative Commons License

[78] G. Frommeyer, U. Brüx, P. Neumann, *ISIJ Int.* **2003**, *43*, 438.
[79] E. O. Hall, *Proc. Phys. Soc., Sect. B* **1951**, *64*, 747.
[80] M. Calcagnotto, D. Ponge, D. Raabe, *Mater. Sci. Eng., A* **2010**, *527*, 7832.
[81] Y. Z. Tian, Y. Bai, L. J. Zhao, S. Gao, H. K. Yang, A. Shibata, Z. F. Zhang, N. Tsuji, *Mater. Charact.* **2017**, *126*, 74.
[82] Y. Bai, Y. Momotani, M. C. Chen, A. Shibata, N. Tsuji, *Mater. Sci. Eng., A* **2016**, *651*, 935.
[83] R. Sandström, *Basic Modeling and Theory of Creep of Metallic Materials*, Springer Nature, Switzerland, Cham **2024**, pp. 131–144, https://doi.org/10.1007/978-3-031-49507-6_7.
[84] Y. Funakawa, T. Shiozaki, K. Tomita, T. Yamamoto, E. Maeda, *ISIJ Int.* **2004**, *44*, 1945.
[85] S. Jiang, H. Wang, Y. Wu, X. Liu, H. Chen, M. Yao, B. Gault, D. Ponge, D. Raabe, A. Hirata, M. Chen, Y. Wang, Z. Lu, *Nature* **2017**, *544*, 460.
[86] M. S. Rashid, *Science* **1980**, *208*, 862.
[87] R. Bjorhovde, *J. Constr. Steel Res.* **2004**, *60*, 393.
[88] S. Liu, X. Rong, H. Guo, R. D. K. Misra, X. Jin, C. Shang, *Mater. Sci. Eng., A* **2021**, *825*, 141783.
[89] L. Kan, Q. Ye, Z. Wang, T. Zhao, *Mater. Sci. Eng., A* **2022**, *855*, 143875.
[90] X. Yang, X. Di, J. Wang, C. Fang, W. Fu, L. Ba, X. Zhou, C. Zhang, C. Li, *Int. J. Plast.* **2023**, *166*, 103654.
[91] A. Ghosh, S. das, S. Chatterjee, *Mater. Sci. Eng., A* **2008**, *486*, 152.
[92] S. K. Dhua, D. Mukerjee, D. S. Sarma, *Metall. Mater. Trans. A* **2001**, *32*, 2259.
[93] S. K. Dhua, A. Ray, D. S. Sarma, *Mater. Sci. Eng., A* **2001**, *318*, 197.
[94] Y. Liu, L. Shi, C. Liu, L. Yu, Z. Yan, H. Li, *Mater. Sci. Eng., A* **2016**, *675*, 371.
[95] A. R. H. Far, S. H. M. Anijdan, S. M. Abbasi, *Mater. Sci. Eng., A* **2019**, *746*, 384.
[96] A. Ghosh, S. Chatterjee, B. Mishra, S. Das, *Metall. Mater. Trans. A* **2005**, *36*, 703.
[97] M. T. Seiyed Beigi, S. R. Hosseini, A. Eshaghi, *Mater. Res. Express* **2019**, *6*, 106514.
[98] J. E. Kim, J. B. Seol, W. M. Choi, B. J. Lee, C. G. Park, *Met. Mater. Int.* **2018**, *24*, 525.
[99] K. Zhang, P. Liu, W. Li, Z. Guo, Y. Rong, *Mater. Sci. Eng., A* **2014**, *619*, 205.
[100] A. Baroutaji, M. Sajjia, A.-G. Olabi, *Thin-Walled Struct.* **2017**, *118*, 137.
[101] I. de Diego-Calderón, D. De Knijf, M. A. Monclús, J. M. Molina-Aldareguia, I. Sabirov, C. Föjer, R. H. Petrov, *Mater. Sci. Eng., A* **2015**, *630*, 27.
[102] J. Rehrl, K. Mraczek, A. Pichler, E. Werner, *Mater. Sci. Eng., A* **2014**, *590*, 360.
[103] M. Calcagnotto, Y. Adachi, D. Ponge, D. Raabe, *Acta Mater.* **2011**, *59*, 658.
[104] H. Kim, J. Lee, F. Barlat, D. Kim, M.-G. Lee, *Acta Mater.* **2015**, *97*, 435.
[105] S. Zhang, K. O. Findley, *Acta Mater.* **2013**, *61*, 1895.
[106] J. Park, M. Kang, S. S. Sohn, S.-H. Kim, H. S. Kim, N. J. Kim, S. Lee, *Mater. Sci. Eng., A* **2017**, *684*, 54.
[107] J.-E. Jin, Y.-K. Lee, *Acta Mater.* **2012**, *60*, 1680.
[108] R. Ueji, N. Tsuchida, D. Terada, N. Tsuji, Y. Tanaka, A. Takemura, K. Kunishige, *Scr. Mater.* **2008**, *59*, 963.
[109] C. X. Huang, G. Yang, C. Wang, Z. F. Zhang, S. D. Wu, *Metall. Mater. Trans. A* **2010**, *42*, 2061.
[110] J. Li, Y. Cao, B. Gao, Y. Li, Y. Zhu, *J. Mater. Sci.* **2018**, *53*, 10442.
[111] B. M. Gonzalez, C. S. B. Castro, V. T. L. Buono, J. M. C. Vilela, M. S. Andrade, J. M. D. Moraes, M. J. Mantel, *Mater. Sci. Eng., A* **2003**, *343*, 51.
[112] G. Frommeyer, U. Brüx, *Steel Res. Int.* **2006**, *77*, 627.
[113] S. S. Sohn, K. Choi, J.-H. Kwak, N. J. Kim, S. Lee, *Acta Mater.* **2014**, *78*, 181.
[114] C. Haase, C. Zehnder, T. Ingendahl, A. Bikar, F. Tang, B. Hallstedt, W. Hu, W. Bleck, D. A. Molodov, *Acta Mater.* **2017**, *122*, 332.
[115] E. D. Moor, J. G. Speer, D. K. Matlock, J.-H. Kwak, S.-B. Lee, *ISIJ Int.* **2011**, *51*, 137.
[116] S. Lee, S.-J. Lee, S. Santhosh Kumar, K. Lee, B. C. D. Cooman, *Metall. Mater. Trans. A* **2011**, *42*, 3638.

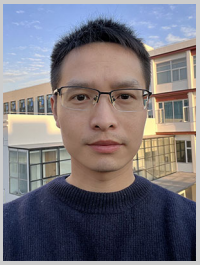

Peikang Xia is a postdoctoral researcher in the School of Materials Science and Engineering at Shanghai Jiao Tong University, China. He received his Ph.D. from Universidad Politécnica de Madrid, Spain, M.S. from Shanghai University, and B.S. from Xi'an University of Technology, China. His current research focuses on the deformation behavior and microstructural mechanisms of advanced high strength steels.

Ilchat Sabirov is a senior researcher in physical simulation and the program leader for advanced manufacturing at IMDEA Materials Institute, Madrid, Spain. He earned his Ph.D. in metallurgy from Montanuniversität Leoben, Austria, in 2004. His current research focuses on alloy and microstructure design in metallic materials to enhance their performance, with an emphasis on industrial applications.

© 2025 Wiley-VCH GmbH

15272648, 0, Downloaded from https://advanced.onlinelibrary.wiley.com/doi/10.1002/adem.202402016 by Technical University Delft, Wiley Online Library on [04/03/2025]. See the Terms and Conditions (https://onlinelibrary.wiley.com/terms-and-conditions) on Wiley Online Library for rules of use; OA articles are governed by the applicable Creative Commons License

Roumen Petrov completed his Ph.D. in 1998 at the Department of Materials Science and Technology, Technical University of Sofia, Bulgaria. From 1983 to 2000, he worked as an associate professor at TU Sofia. Since 2000, he has been affiliated with Ghent University, Belgium, where he currently holds the position of senior full professor. Additionally, since 2005, he has served as a part-time researcher and later as an associate professor at TU Delft, The Netherlands. His research focuses on the microstructural design of steel and non-ferrous alloys, as well as the characterization of their microstructure and properties using advanced characterization techniques.

Patricia Verleysen is full-time professor at Ghent University (Belgium) in the research group Materials Science and Technology (MST). Within MST, Patricia Verleysen established DyMaLab to group the activities on the impact-dynamic behavior of materials and structures (see https://mst.ugent.be/dymalab/research/). A key expertise of the DyMaLab group is the development of dedicated experimental methodologies to identify the strain rate-dependent properties of materials. She is also involved in modeling activities, again with a strong focus on strain rate and temperature-dependent deformation and damage of materials. The research results are published in more than 130 peer-reviewed journal papers.

© 2025 Wiley-VCH GmbH

15272648, 0, Downloaded from https://advanced.onlinelibrary.wiley.com/doi/10.1002/adem.202402016 by Technical University Delft, Wiley Online Library on [04/03/2025]. See the Terms and Conditions (https://onlinelibrary.wiley.com/terms-and-conditions) on Wiley Online Library for rules of use; OA articles are governed by the applicable Creative Commons License